INTERNATIONAL JOURNAL FOR NUMERICAL METHODS IN FLUIDS
Int. J. Numer. Meth. Fluids 2009; **61**:995–1028
Published online 11 February 2009 in Wiley InterScience (www.interscience.wiley.com). DOI: 10.1002/fld.1993

Particle trajectory calculations with a two-step three-time level semi-Lagrangian scheme well suited for curved flows

Ricardo Carvalho de Almeida[1,*,†], Giovana Araújo Siqueira Costa[2], Luiz Claudio Monteiro da Fonseca[2] and José Luis Drummond Alves[2]

[1]*Laboratory for Environmental Monitoring and Modeling Analysis, Federal University in Paraná, Curitiba, Brazil*
[2]*Graduate School and Research in Engineering, Civil Engineering Program, Federal University in Rio de Janeiro, Rio de Janeiro, Brazil*

SUMMARY

This study proposes a new two-step three-time level semi-Lagrangian scheme for calculation of particle trajectories. The scheme is intended to yield accurate determination of the particle departure position, particularly in the presence of significant flow curvature. Experiments were performed both for linear and non-linear idealized advection problems, with different flow curvatures. Results for simulations with the proposed scheme, and with three other semi-Lagrangian schemes, and with an Eulerian method are presented. In the linear advection problem the two-step three-time level scheme produced smaller root mean square errors and more accurate replication of the angular displacement of a Gaussian hill than the other schemes. In the non-linear advection experiments the proposed scheme produced, in general, equal or better conservation of domain-averaged quantities than the other semi-Lagrangian schemes, especially at large Courant numbers. In idealized frontogenesis simulations the scheme performed equally or better than the other schemes in the representation of sharp gradients in a scalar field. The two-step three-time level scheme has some computational overhead as compared with the other three semi-Lagrangian schemes. Nevertheless, the additional computational effort was shown to be worthwhile, due to the accuracy obtained by the scheme in the experiments with large time steps. The most remarkable feature of the scheme is its robustness, since it performs well both for small and large Courant numbers, in the presence of weak as well strong flow curvatures. Copyright © 2009 John Wiley & Sons, Ltd.

Received 31 October 2007; Revised 27 November 2008; Accepted 29 November 2008

KEY WORDS: Lagrangian; partial differential equations; explicit time integration; stability; finite difference methods; hyperbolic equations

*Correspondence to: Ricardo Carvalho de Almeida, Universidade Federal do Paraná, Centro Politécnico, Caixa Postal 19022, CEP 81531-980, Curitiba - PR, Brazil.
†E-mail: rcalmeida@ufpr.br, rcalmeidabr@terra.com.br

1. INTRODUCTION

As computational resources have become more powerful, numerical weather prediction models have rapidly advanced to represent smaller scales of atmospheric motions. Global models are reaching mesoscale resolution and more detailed structures have been able to be represented by those models. Even though the cost of high performance computers has become lower in time, there is still a need for efficient numerical methods that will take full advantage of these new platforms, without compromising the accuracy in the replication of complex and detailed flow structures.

Following the pioneering works of Wiin-Nielsen [1] and Sawyer [2], Robert [3] proposed the semi-Lagrangian method, which has been recognized as an efficient technique to be employed in atmospheric models, which allows for the use of time steps longer than those limited by the Courant–Friedrichs–Levy (CFL) condition. The main feature of the method is the use of the Lagrangian frame of reference, where the material derivatives of the dependent variables are calculated in the model equations by following the trajectory of the fluid particles. In the semi-Lagrangian method the final position of a fluid particle is coincident with a grid point, and the trajectory of a fluid particle is calculated with the use of some backward in time numerical scheme. Therefore, the method combines the advantage of a regular distribution of the grid points in the model domain characteristic of Eulerian methods, with unconditional numerical stability with respect to advection of Lagrangian methods.

One of the problems of the semi-Lagrangian method pointed out by Purser and Leslie [4] is the difficulty in accurately determining the departure points of the trajectories of fluid particles in regions where the flow is strongly curved, when using long time steps. This paper addresses this problem, by proposing a new semi-Lagrangian scheme which intends to improve the accuracy of the computation of the trajectory of the fluid particles, particularly in situations where there is a pronounced curvature in the flow.

In Section 2 some background information on the semi-Lagrangian method is presented, as well as the details of the proposed two-step three-time level scheme. Section 3 describes the problems that will be used to evaluate the performance of the scheme. The results of the numerical experiments performed with the use the proposed scheme and with three other semi-Lagrangian schemes are analyzed in Section 4. Section 5 discusses the results and presents the conclusions of the study.

2. THE SEMI-LAGRANGIAN METHOD

2.1. Background

The semi-Lagrangian method was initially applied to the numerical solution of weather forecasting problems based on the vorticity conservation equation

$$\frac{\mathrm{D}\eta}{\mathrm{D}t}=0 \tag{1}$$

where η is the absolute vorticity. Equation (1) expresses that η is conserved following the fluid particles i.e. in the Lagragian frame of reference. Winn-Nielsen [1] was the first to propose a method to integrate (1) in Lagrangian coordinates but he found a serious problem, that was the rapid distortion of an initially uniform computational domain. Sawyer [2] proposed then that

DOI: 10.1002/fld

the fluid elements that would be followed along the flow would be changed during the integration, eliminating the ones that moved out of the domain and including new particles to keep a complete representation of the domain. This method was called semi-Lagrangian. In both aforementioned methods the future positions of the fluid particles had to be determined to allow for the calculation of the material derivative expressed by (1).

Robert [3] introduced a variation to Sawyer's semi-Lagrangian method by which the future positions of the fluid particles were coincident with the grid points and their positions in the previous time step were calculated, using a backward in time scheme. With this change the advantage of a regular distribution of fluid elements characteristic of Eulerian methods could be associated with the computational efficiency of the Lagrangian methods.

In three-time level schemes the material derivative of a variable q is calculated by using the following approximation:

$$\frac{\mathrm{D}q}{\mathrm{D}t} \cong \frac{q(\mathbf{r}(t+\Delta t), t+\Delta t) - q(\mathbf{r}(t-\Delta t), t-\Delta t)}{2\Delta t} \tag{2}$$

In two-time level schemes the material derivative is approximated as

$$\frac{\mathrm{D}q}{\mathrm{D}t} \cong \frac{q(\mathbf{r}(t+\Delta t), t+\Delta t) - q(\mathbf{r}(t), t)}{\Delta t} \tag{3}$$

In both the schemes, $\mathbf{r}(t+\Delta t)$ is the position vector of the fluid particle at time $t+\Delta t$, which is chosen to be coincident with a grid point.

Durran [5] presents a detailed analysis of the stability properties of the two-time level scheme (3) showing that the scheme is unconditionally stable with respect to advection. Robert [3] demonstrated that the three-time level scheme of Equation (2) is also unconditionally stable. Another feature of the semi-Lagrangian method pointed out by Durran is that it prevents the occurrence of non-linear instability due to aliasing, since the non-linear advective terms are not explicitly represented in the Lagrangian frame of reference.

The accuracy of the semi-Lagrangian method will depend on errors introduced in two stages of its implementation: the determination of the departure point of the trajectory of the fluid particle and the interpolation of the value of the variable at that position which, in general, will not coincide with a grid point position. However, the semi-Lagrangian method behaves differently from Eurelian methods, since error is not monotonic with respect to time step size Δt. The overall error of semi-Lagrangian schemes has the form [6]

$$O\left(\Delta t^k + \frac{\Delta x^{p+1}}{\Delta t}\right) \tag{4}$$

where k is the order of the time integration scheme and p is the order of the spatial interpolation.

According to (4) as Δt increases, the number of interpolations needed to integrate the equations for a certain time interval decreases. If the second term is the dominating one, the overall error will decrease for larger time steps. On the other hand, as Δt increases, the first term in (4) may become the dominating one and in that case the overall error will increase for increasing Δt.

Purser and Leslie [4] point out that in situations where the flow is strongly curved, the semi-Lagrangian approach does not perform well due to the fact that the location of the particle departure point is subject to time truncation errors, even when high-order accuracy spatial discretization is employed. They state that several methods have been proposed to reduce the truncation error

DOI: 10.1002/fld

in time and most of them take the form of backward in time high-order extrapolations. Those methods, however, should not be expected to be as accurate as those using time interpolations from solutions at both end points of each trajectory.

Several authors have proposed two- and three-time level schemes for calculation of fluid particle trajectories. Durran [5] and Staniforth and Côté [7] present reviews of many of them. In this study three recognized schemes will be used as reference for comparison with the proposed two-step three-time level scheme, as follows.

2.2. Robert three-time level scheme

Robert [3] introduced a three-time level scheme for the calculation of the fluid particle trajectories (hereafter SL3T). In two-dimensions, the position of a fluid particle at time $t+\Delta t$, which is coincident with a grid point (i, j), is represented as

$$\mathbf{r}(t+\Delta t)=(x_i, y_j) \tag{5}$$

and the approximation for Equation (3) will be

$$\frac{\mathrm{D}q}{\mathrm{D}t}\cong\frac{q(x_i, y_j, t+\Delta t)-q(x_i-2a, y_j-2b, t)}{2\Delta t} \tag{6}$$

where a and b are the particle displacements along the x and y directions, respectively, during time interval Δt. Those displacements are calculated with the iterative procedure

$$a^{m+1}=\Delta t\cdot u(x_i-a^m, y_j-b^m, t) \tag{7a}$$

$$b^{m+1}=\Delta t\cdot v(x_i-a^m, y_j-b^m, t) \tag{7b}$$

where m is the mth iteration, and u and v are the velocity components along the x and y directions, respectively, at time t.

Pudykiewicz and Staniforth [8] showed that the necessary condition for convergence of the iterative procedure of Equations (7) is

$$\Delta t\cdot\max\left(\left|\frac{\partial u}{\partial x}\right|, \left|\frac{\partial u}{\partial y}\right|, \left|\frac{\partial v}{\partial x}\right|, \left|\frac{\partial v}{\partial y}\right|\right)<1 \tag{8}$$

Kuo and Williams [9] point out that convergence can be obtained with no more than three iterations. Robert [3] compared the use of two and four iterations in his atmospheric model and did not find any significant differences in the results.

A disadvantage of this method is the occurrence of noise due to the existence of a computational mode in the solution.

2.3. McDonald and Bates two-time level scheme

McDonald and Bates [10] (hereafter SL2T) proposed the following two-time level scheme, based on the use of the particle velocity at time $t+\Delta t/2$

$$\frac{\mathrm{D}q}{\mathrm{D}t}\cong\frac{q(x_i, y_j, t+\Delta t)-q(x_i-a, y_j-b, t)}{\Delta t} \tag{9}$$

DOI: 10.1002/fld

with

$$a^{m+1} = \Delta t \cdot u^* \left(x_i - \frac{a^m}{2}, y_j - \frac{b^m}{2}, t + \frac{\Delta t}{2} \right) \tag{10a}$$

$$b^{m+1} = \Delta t \cdot v^* \left(x_i - \frac{a^m}{2}, y_j - \frac{b^m}{2}, t + \frac{\Delta t}{2} \right) \tag{10b}$$

Since u and v are not known at $t + \Delta t/2$, the following extrapolation in time procedure is used:

$$u^* \left(\mathbf{r}\left(t + \frac{\Delta t}{2} \right), t + \frac{\Delta t}{2} \right) = \frac{3}{2} u \left(\bar{r}\left(t + \frac{\Delta t}{2} \right), t \right) - \frac{1}{2} u \left(\mathbf{r}\left(t + \frac{\Delta t}{2} \right), t - \Delta t \right) \tag{11a}$$

$$v^* \left(\mathbf{r}\left(t + \frac{\Delta t}{2} \right), t + \frac{\Delta t}{2} \right) = \frac{3}{2} v \left(\bar{r}\left(t + \frac{\Delta t}{2} \right), t \right) - \frac{1}{2} v \left(\mathbf{r}\left(t + \frac{\Delta t}{2} \right), t - \Delta t \right) \tag{11b}$$

The procedure is implemented with one iteration only. The authors claim that their method is as accurate as the SL3T scheme, and yet more efficient, since it requires less spatial interpolations. However, Bates *et al.* [11] observed the occurrence of spurious gravity waves in their shallow water atmospheric model that employed the SL2T scheme. They believed that the problem was caused by the evaluation of the non-linear term of the continuity equation by using the extrapolation procedure of Equations (10). Staniforth and Côté [7] point out that this problem occurs when the non-linear terms of the equations of motion that involve self-advection of momentum are evaluated with the use of temporal extrapolations.

2.4. Hortal stable two-time level scheme

In order to overcome the instability problem of the SL2T scheme, which appeared as noise in forecast fields of the ECMWF semi-Lagrangian model, Hortal [12] developed the following stable two-time level scheme (hereafter SL2TS):

$$\frac{\mathrm{D}q}{\mathrm{D}t} \cong \frac{q(x_i, y_j, t + \Delta t) - q(x_i - a, y_j - b, t)}{\Delta t} \tag{12a}$$

with

$$a^{m+1} = \frac{\Delta t}{2} [(2u^*(x_i - a^m, y_j - b^m, t) - u^*(x_i - a^m, y_j - b^m, t - \Delta t)) + u(x_i, y_j, t)] \tag{12b}$$

$$b^{m+1} = \frac{\Delta t}{2} [(2v^*(x_i - a^m, y_j - b^m, t) - v^*(x_i - a^m, y_j - b^m, t - \Delta t)) + v(x_i, y_j, t)] \tag{12c}$$

The method uses the idea that the fluid particles are displaced along their trajectories in a uniformly accelerated movement. In that case, the middle point of the trajectory is not at the same point of the average between the departure and the arrival points. The total time derivative of the velocity is assumed to be constant and it is estimated by using velocity values at the arrival and departure points, different from the SL2T scheme that uses estimates at the midpoint of the trajectory. The SL2TS scheme was implemented in the ECMWF operational model and the noise problem in the forecasts was successfully eliminated.

DOI: 10.1002/fld

2.5. The two-step three-time level scheme

In two of the aforementioned schemes for determination of the particle departure point, the velocity is kept constant during one time step (between t and $t+\Delta t$ for SL2T, and between $t-\Delta t$ and $t+\Delta t$ for SL3T), and in the SL2TS scheme the particle acceleration is assumed to be constant. The main feature of the proposed two-step three-time level scheme (hereafter SL2S3T) is to allow both for the velocity and the acceleration vectors of the particles to vary between $t-\Delta t$ and $t+\Delta t$. The scheme is based upon the general idea of multistage methods [5], where each integration step requires the estimate of the dependent variable at several intermediate times. After obtaining those intermediate values, a final estimate of the predicted variable is obtained. An example of Eulerian multistage methods is the family of Runge–Kutta schemes. The rationale behind the proposed semi-Lagrangian scheme is to 'break' the particle trajectory into two steps. In the first step, starting from grid point (i, j), at time $t+\Delta t$, the particle is displaced backwards for a time interval Δt with the velocity calculated at an intermediate position (x^*, y^*) for time t. In the second step, starting from the particle position at time t calculated in the previous step, the particle is displaced backwards for another Δt, with the velocity calculated for the intermediate position (x^{**}, y^{**}), also for time t. The intermediate positions (x^*, y^*) and (x^{**}, y^{**}) are obtained by considering displacements of the particle for a time interval $\Delta t/2$.

The scheme can be expressed by the following equations:

$$\frac{\mathrm{D}q}{\mathrm{D}t} \cong \frac{q(x_i, y_j, t+\Delta t) - q(x'', y'', t-\Delta t)}{2\Delta t} \tag{13}$$

where

1st step:

$$a^{*(m+1)} = \frac{\Delta t}{2} u(x_i - a^{*(m)}, y_j - b^{*(m)}, t) \tag{14a}$$

$$b^{*(m+1)} = \frac{\Delta t}{2} v(x_i - a^{*(m)}, y_j - b^{*(m)}, t) \tag{14b}$$

$$x' = x_i - 2a^* \tag{14c}$$

$$y' = y_j - 2b^* \tag{14d}$$

and

2nd step:

$$a^{**(m+1)} = \frac{\Delta t}{2} u(x' - a^{**(m)}, y' - b^{**(m)}, t) \tag{15a}$$

$$b^{**(m+1)} = \frac{\Delta t}{2} v(x' - a^{**(m)}, y' - b^{**(m)}, t) \tag{15b}$$

$$x'' = x' - 2a^{**} \tag{15c}$$

$$y'' = y' - 2b^{**} \tag{15d}$$

Notice that although at each step the particle is displaced for a time interval Δt, only spatial interpolations are used, and the particle velocities refer to time t. In this way it is expected that

DOI: 10.1002/fld

in situations where a rapid change in the velocity vector occurs during the time interval $2\Delta t$ the particle is being displaced, the 'broken' trajectory will be able to more realistically represent such changes when long time steps are used.

The time truncation error of the scheme can be evaluated by using the analysis procedure described in Durran [5] as reference. We consider one dimension only. It is important to point out that the following analysis does not consider interpolation errors, only truncation errors are considered.

Let the estimated position of a fluid particle at time t^n be $\tilde{x}^n(t^n)$. We define the particle displacements as

1st step:

$$\Delta s_1 = x_j - \tilde{x}_j^n = \Delta t \cdot u(x^{n+1/2}, t^n) \tag{16a}$$

2nd step:

$$\Delta s_2 = \tilde{x}_j^n - \tilde{x}_j^{n-1} = \Delta t \cdot u(x^{n-1/2}, t^n) \tag{16b}$$

where $x_j = x^{n+1}$ is the particle position at time t^{n+1}, which corresponds to grid point j. Notice that the displacement velocities are referred to the intermediate time t^n. The backward trajectory is computed from position x_j with the following expression:

$$\tilde{x}_j^{n-1}(t^{n-1}) = x^{n+1} - \Delta s_1 - \Delta s_2 \tag{17}$$

We expand $u(x^{n+1/2}, t^n)$ and $u(x^{n-1/2}, t^n)$ in the Taylor series about the estimated intermediate position $\tilde{x}_j^n(t^n)$

$$u(x^{n+1/2}, t^n) = u^n + \frac{\Delta s_1}{2}\frac{\partial u}{\partial x}(\tilde{x}_j^n, t^n) + O(\Delta s_1^2) \tag{18a}$$

$$= u^n + \frac{1}{2}\frac{\partial u}{\partial x}(\tilde{x}_j^n, t^n) \cdot \Delta t[u^n + O(\Delta t)] + O(\Delta t^2) \tag{18b}$$

$$= u^n + u\frac{\partial u}{\partial x}(\tilde{x}_j^n, t^n)\frac{\Delta t}{2} + O(\Delta t^2) \tag{18c}$$

$$u(x^{n-1/2}, t^n) = u^n - \frac{\Delta s_2}{2}\frac{\partial u}{\partial x}(\tilde{x}_j^n, t^n) + O(\Delta s_2^2) \tag{18d}$$

$$= u^n - \frac{1}{2}\frac{\partial u}{\partial x}(\tilde{x}_j^n, t^n) \cdot \Delta t[u^n - O(\Delta t)] + O(\Delta t^2) \tag{18e}$$

$$= u^n - u\frac{\partial u}{\partial x}(\tilde{x}_j^n, t^n)\frac{\Delta t}{2} + O(\Delta t^2) \tag{18f}$$

Equalities (18b) and (18e) were obtained by substituting (16a) and (16b) into (18a) and (18d), respectively.

Introducing (18c) and (18f) into (17) yields

$$\tilde{x}_j^{n-1}(t^{n-1}) = x^{n+1} - 2u^n\Delta t - O(\Delta t^3) = x^{n+1} - 2\left(\frac{\mathrm{d}x}{\mathrm{d}t}\right)^n \Delta t - O(\Delta t^3) \tag{19}$$

DOI: 10.1002/fld

Expression (19) states that the local truncation error introduced in each step of the calculation of the departure position is $O(\Delta t^3)$. Therefore, the global truncation error of the approximation of the trajectory equation of the SL2S3T scheme will be $O(\Delta t^2)$, since

$$\left(\frac{\mathrm{d}x}{\mathrm{d}t}\right)^n = \frac{x^{n+1} - \tilde{x}_j^{n-1}(t^{n-1})}{2\Delta t} - O(\Delta t^2) \tag{20}$$

The time truncation errors of the SL2T, SL2TS and the SL3T schemes are also $O(\Delta t^2)$ [7, 12].

3. TEST PROBLEMS

3.1. The linear advection problem

The first problem that will be used to evaluate the SL2S3T scheme will be the uniform circular translation without diffusion of a function $\phi(x, y, t)$. It has been already used by Pudykiewicz and Staniforth [8] in the evaluation of the SL3T scheme. The governing equation is

$$\frac{\mathrm{D}\phi}{\mathrm{D}t} = 0 \tag{21}$$

and $\phi(x, y, t)$ is a Gaussian hill, centered at (x_0, y_0), defined as [13]

$$\phi(x, y) = A_0 \exp[(R/2\Delta x)^2] \tag{22}$$

where $R^2 = (x - x_0)^2 + (y - y_0)^2$ is the radius of the hill base, A_0 is the concentration distribution, and Δx is the grid spacing (which equals Δy).

The center of the Gaussian hill moves around the center of the domain with constant angular velocity $\omega = V_\mathrm{t}/R_\mathrm{a}$, where V_t is the tangential velocity of the hill base center point (x_0, y_0) and R_a is the advection radius, that is, the distance between the domain center and the hill base center point. Since the angular velocity is prescribed, the simulation results will be controlled by the analytical solution.

3.2. The non-linear advection problem

The second problem that will be used to evaluate the SL2S3T scheme uses Arakawa and Lamb [14] as reference. It consists of simulating a horizontal non-divergent flow, governed by the relative vorticity (ζ) conservation equation

$$\frac{\mathrm{D}\zeta}{\mathrm{D}t} = 0 \tag{23}$$

which is defined in terms of the streamfunction ψ with

$$u = -\frac{\partial \psi}{\partial y} \tag{24a}$$

$$v = \frac{\partial \psi}{\partial x} \tag{24b}$$

$$\zeta = \nabla^2 \psi \tag{24c}$$

where ∇^2 is the horizontal Laplacian operator.

DOI: 10.1002/fld

In its Eulerian form, Equation (23) can be written as

$$\frac{\partial \zeta}{\partial t} = J(\zeta, \psi) \tag{25}$$

where J is the Jacobian operator, defined as

$$J(\zeta, \psi) = \frac{\partial \zeta}{\partial x}\frac{\partial \psi}{\partial y} - \frac{\partial \zeta}{\partial y}\frac{\partial \psi}{\partial x} \tag{26}$$

The Jacobian operator (26) has the following integral properties:

$$\overline{J(\zeta, \psi)} = 0 \tag{27a}$$

$$\overline{\zeta J(\zeta, \psi)} = 0 \tag{27b}$$

$$\overline{\psi J(\zeta, \psi)} = 0 \tag{27c}$$

The overbar represents the domain average of a quantity, which by definition has ψ constant along its boundary. Properties (27a)–(27c) imply that the mean vorticity $\bar{\zeta}$, the mean enstrophy $\overline{\zeta^2}/2$, and the mean kinetic energy (per unit mass) $\overline{|\nabla\psi|^2}/2$ will be conserved with time. Therefore, it is desirable that a discretization scheme conserves those properties.

In order to avoid non-linear instability caused by aliasing, Arakawa and Lamb [14] developed the following spatial discretization scheme for Eulerian finite difference integration schemes, which formally conserves the quantities defined by expressions (27a)–(27c)

$$J(\zeta, \psi) = \frac{J_1 + J_2 + J_3}{3} \tag{28a}$$

$$J_1 = (\Delta_x \zeta)(\Delta_y \psi) - (\Delta_y \zeta)(\Delta_x \psi) \tag{28b}$$

$$J_2 = \Delta_y(\psi \Delta_x \zeta) - \Delta_x(\psi \Delta_y \zeta) \tag{28c}$$

$$J_3 = \Delta_x(\zeta \Delta_y \psi) - \Delta_y(\zeta \Delta_x \psi) \tag{28d}$$

where

$$\Delta_x q = \frac{q_{i+1,j} - q_{i-1,j}}{2\Delta x} \tag{29a}$$

$$\Delta_y q = \frac{q_{i,j+1} - q_{i,j-1}}{2\Delta y} \tag{29b}$$

where i, j are the grid point indices along the x and y directions, respectively.

The semi-Lagrangian schemes in this study do not formally conserve any of the quantities (27a)–(27c). Nevertheless, it is desirable to assess conservation characteristics of numerical schemes in order to evaluate its suitability to atmospheric numerical simulations, especially for long ones, such as those preformed in climate studies. The non-linear advection test problem presented here will allow for the assessment of the conservation properties of the different semi-Lagrangian schemes.

DOI: 10.1002/fld

3.3. The idealized frontogenesis problem

Kuo and Williams [9] state that there are many important atmospheric phenomena associated with sharp spatial gradients, such as frontogenesis and the formation of discontinuities from unbalanced initial conditions. The numerical solution for those scale-collapse problems requires the use of computational methods that have the ability to accurately represent very sharp gradients. Also, numerical errors caused by the presence of those gradients should not contaminate the smooth solution away from the collapse region. In their paper the authors verified that semi-Lagrangian schemes perform well in simulating scale-collapse problems with the use of long time steps.

The idealized frontogenesis problem of Doswell [15] is an appropriate test for the semi-Lagrangian schemes presented in this paper, since it allows for the assessment of the ability of the schemes to handle strong gradients in the presence of strongly curved flow. The problem consists of a wind field produced by a steady state, two-dimensional, nondivergent vortex with a purely tangential wind field V_T, which is a function of the distance from the origin r, according to

$$V_T(r) = \frac{\tanh r}{\cosh^2 r} \tag{30}$$

With the wind field defined by (30), the x and y components of the flow are

$$u(x, y) = -V_T(r) \sin\theta \tag{31a}$$

$$v(x, y) = V_T(r) \cos\theta \tag{31b}$$

with $\theta = \tan^{-1}(y/x)$ and $r = (x^2 + y^2)^{1/2}$.

A scalar field is superimposed on the wind field and is linearly advected by it. Doswell [15] used the following initial scalar field:

$$Q(x, y) = -\tanh y \tag{32}$$

An interesting feature of this problem is that even though the wind field is nondivergent, the scalar field converges to the center of the wind field in an inward spiraling frontal pattern. That causes a continuous increase of the spatial gradients of the scalar field, while the fluid particles are advected by the circular wind field.

There are two important characteristics of this problem that will be objectively analyzed in the experiments: the scalar field remains antisymmetric in time, therefore, the average value of the scalar field must be constant equal to zero; and, as demonstrated by Davies-Jones [16], at the origin, $|\nabla Q| = 1$ for all times.

4. NUMERICAL EXPERIMENTS AND RESULTS

4.1. Linear advection experiments

In this study we are particularly interested in assessing the effects of flow curvature on the performance of the semi-Lagrangian schemes. Three domains were set for the numerical experiments. The one with smaller flow curvatures had a mesh with 99×99 grid points and $R_a = 25\Delta x$; an intermediate curvature domain was set with 67×67 grid points and $R_a = 17\Delta x$; and a domain with larger curvature was set with 33×33 grid points and $R_a = 8\Delta x$. For all experiments, $A_0 = 10^5$ and

DOI: 10.1002/fld

$\Delta x = \Delta y = 10^5$ m. With those parameters the function ϕ ranges from 0 to 10^5. The angular velocity for each domain was set to produce a tangential speed of the hill center $|V_t| = 10$ m/s.

Experiments were performed with the Gaussian hill rotating around the domain center, with the time step Δt adjusted to produce Courant numbers $C = 1.0$, 2.0, 4.0, 6.0, 8.0 and 10.0, calculated by

$$C = \frac{|V_{MAX}|\Delta t}{\Delta x\sqrt{2}} \tag{33}$$

where $|V_{MAX}|$ is the maximum speed occurring at a grid point of the domain.

Each scheme was implemented with the iterative procedure to calculate the length of the particle displacement with two iterations at most. If after the first iteration the precision of the calculated length was equal or better than 0.1% the second iteration was not necessary. Bicubic spatial interpolations were used in all experiments in the interior of the domains and bilinear interpolations along the boundaries.

For reference, Eulerian integrations using the *leapfrog* scheme (centered in space and time) [17], with Courant number equal to 1.0 were performed. This numerical scheme has $O(\Delta t^2)$ truncation error, so it is appropriate for comparison with the semi-Lagrangian schemes presented in this study, which are also $O(\Delta t^2)$ accurate.

Table I presents the root mean square (RMS) errors of the ϕ function [Equation (22)] for the experiments with Courant number 1.0, after 1 and 10 revolutions. Results for the Eulerian method are not presented for 10 revolutions because the simulation became unstable before reaching that number of revolutions. It is clear that the Eulerian method presents significantly greater errors than the semi-Lagrangian schemes, for all grids, after one revolution of the Gaussian hill. The following analysis, therefore, will focus on only the semi-Lagrangian schemes.

Figure 1 presents the RMS errors of ϕ as a function of the Courant number, after one, two, four, and 10 revolutions of the Gaussian hill, obtained from the comparison of the analytical and numerical solutions of the experiments with the 99×99 grid points domain. There is a general tendency of the errors to decrease with increasing Δt for the SL2T, the SL2TS and the SL2S3T schemes. For the SL3T scheme the RMS errors decrease for Courant numbers less than 6.0 and increase for values greater than that. These results are due to the nonmonotonic behavior of the error in the semi-Lagrangian method, expressed by Equation (4). It can be seen that SL3T scheme is more sensitive to cumulative time truncation errors, since the RMS error grows more rapidly than for the other schemes for larger periods of integration. The simulations with the SL2T and

Table I. Root mean square errors of the ϕ function after one and 10 revolutions of the Gaussian hill for experiments with Courant number equal to 1.0, with the three computational domains.

Mesh	Eulerian	SL2T	SL2TS	SL3T	SL2S3T
Results after 1 revolution ($\times 10^4$)					
99×99	1.473	0.157	0.157	0.148	0.148
67×67	1.465	0.211	0.212	0.197	0.197
33×33	1.457	0.342	0.342	0.310	0.310
Results after 10 revolutions ($\times 10^4$)					
99×99	—	0.216	0.216	0.212	0.212
67×67	—	0.309	0.309	0.302	0.302
33×33	—	0.577	0.577	0.557	0.556

DOI: 10.1002/fld

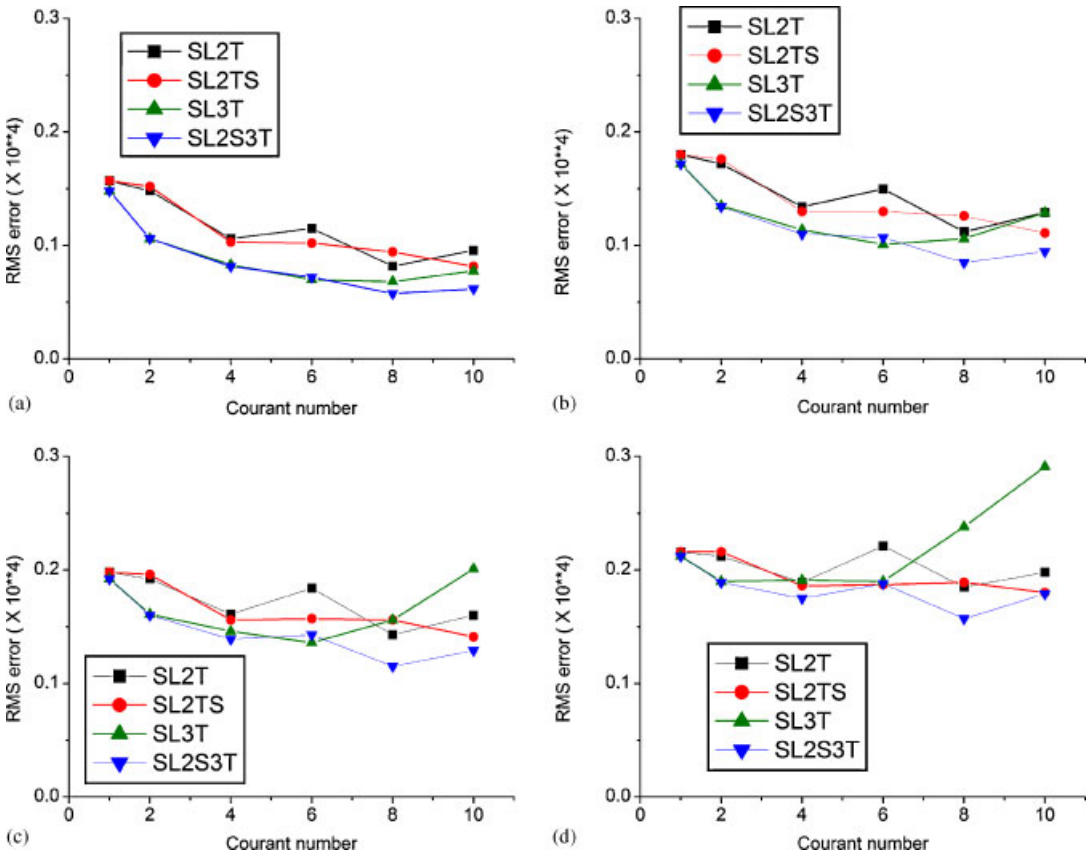

Figure 1. Root mean square (RMS) error of ϕ as a function of the Courant number after one (a), two (b), four (c), and 10 (d) revolutions of the Gaussian hill, for the experiments with the 99×99 grid points mesh.

the SL2TS schemes have larger errors than those with the SL3T and the SL2S3T schemes for shorter periods of integration and small Courant numbers. Overall, the SL2S3T scheme produces equal or smaller RMS errors than the other schemes for the 99×99 grid.

Figure 2 shows the RMS errors of ϕ for the experiments with the intermediate flow curvature domain, with 67×67 grid points. Again, the SL2S3T scheme performs equally or better than the other schemes in all cases, and the SL3T scheme is more sensitive to time truncation errors than the other schemes for larger Courant numbers. In this case the errors produced by the SL3T scheme started growing for Courant numbers greater than 4.0, instead of 6.0 as occurred in the 99×99 grid points mesh.

The RMS errors of ϕ obtained in the experiments with the 33×33 grid points domain, which displays a more strongly curved flow, are presented in Figure 3. In this case all schemes show an initial decrease followed by an increase in the RMS error, for increasing Δt. The SL3T scheme is more sensitive to time truncation errors, since for Courant numbers greater than 2.0 the RMS error increases very fast with increasing Δt. The SL3T scheme is also the one where cumulative errors are more significant. In this case the SL2S3T scheme also performs equally or better than

DOI: 10.1002/fld

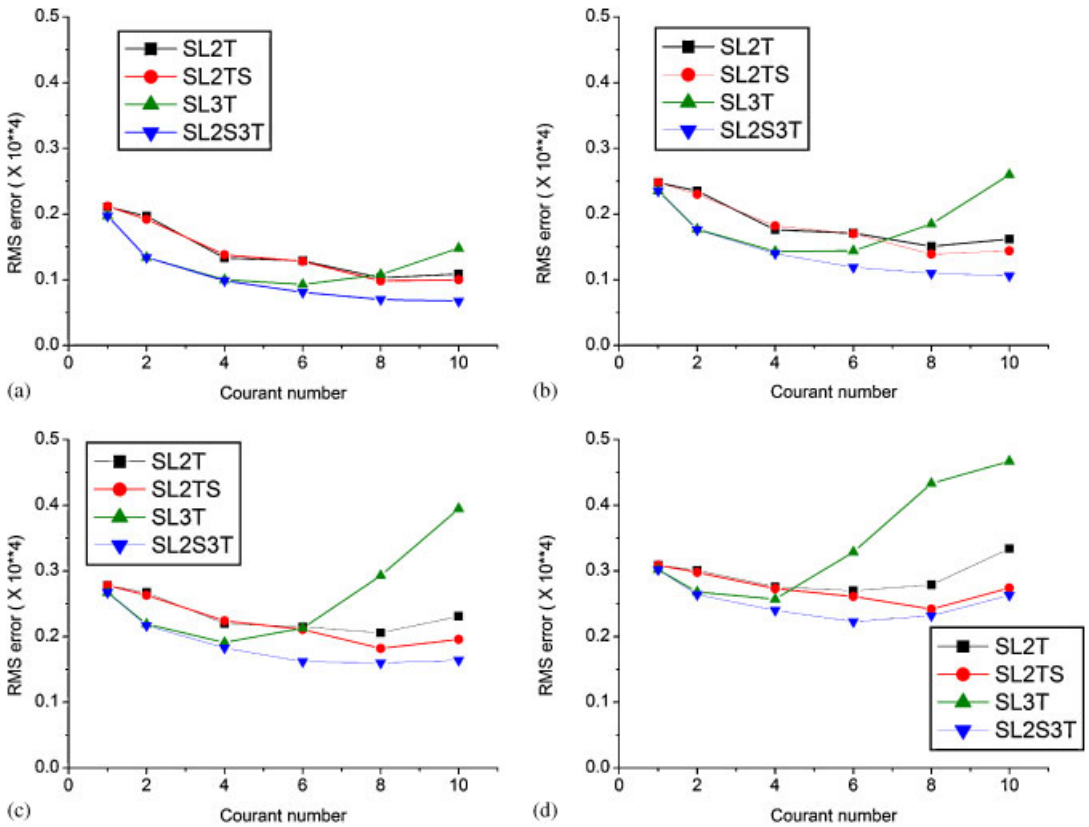

Figure 2. Root mean square (RMS) error of ϕ as a function of the Courant number after one (a), two (b), four (c), and 10 (d) revolutions of the Gaussian hill, for the experiments with the 67×67 grid points mesh.

the SL2T and the SL3T schemes in all cases. The SL2TS scheme has RMS errors smaller than the SL2S3T scheme only for very large Courant numbers, after 10 revolutions.

Notice that the SL3T and the SL2S3T schemes show approximately equal errors for Courant numbers 1.0 and 2.0 in all experiments. Also, it is apparent that the RMS errors increase for increasing flow curvature.

Following Pudykiewicz and Staniforth [8] accuracy and conservation properties of the schemes were also analyzed. Tables II–IV present the values of the following quantities calculated for the experiments with the 99×99, the 67×67, and the 33×33 grid points meshes, respectively, for experiments with Courant numbers 1.0, 4.0, and 10.0, after one and 10 revolutions: the maximum (ϕ_{MAX}) and minimum (ϕ_{MIN}) values of the ϕ function, to evaluate numerical dispersion; the ratio of the sum of the grid point values of ϕ to the initial sum ($\sum \phi_{ij} / \sum \phi_{ij}(0)$), to evaluate conservation of the ϕ field ('mass' conservation); percentual loss of ϕ, defined as 1 minus the ratio of the sum of the squares of the grid point values of ϕ at a certain time to the sum of the squares of the initial values of $\phi[1-(\sum \phi_{ij}^2 / \sum \phi_{ij}^2(0))]$, to assess the amplification/damping properties of the schemes. The tables also present the correlation between the values of ϕ produced by the

DOI: 10.1002/fld

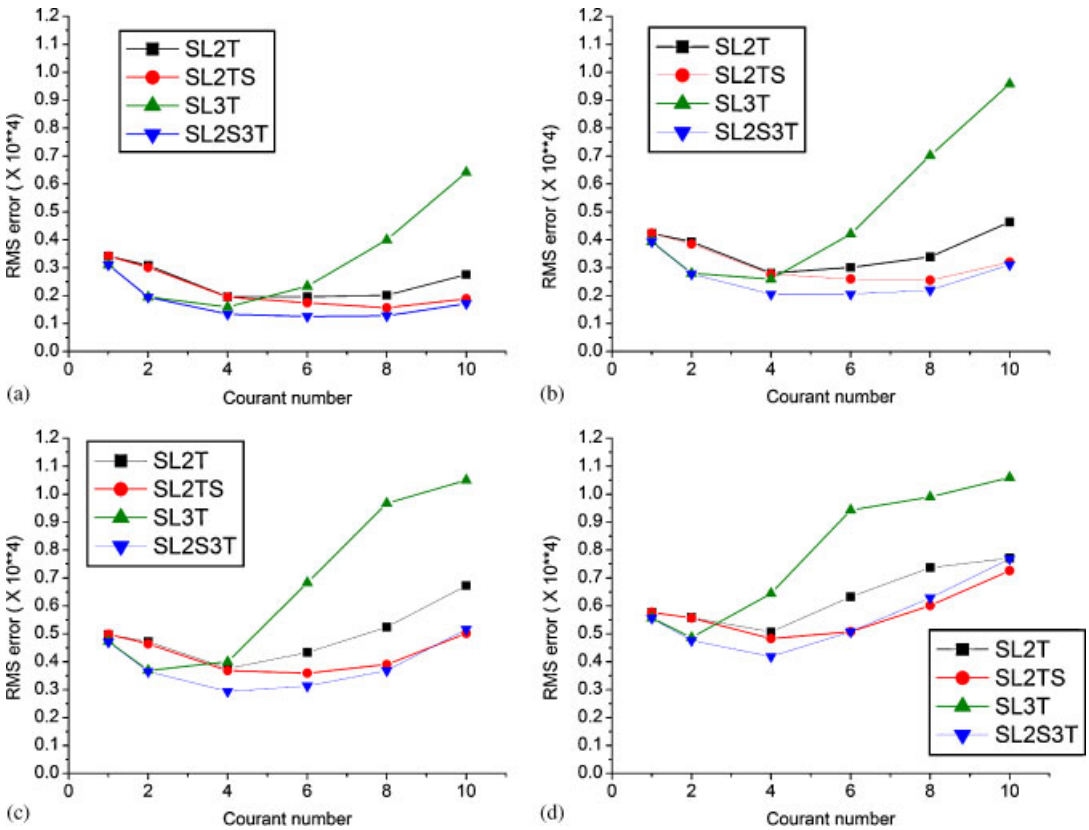

Figure 3. Root mean square (RMS) error of ϕ as a function of the Courant number after one (a), two (b), four (c), and 10 (d) revolutions of the Gaussian hill, for the experiments with the 33×33 grid points mesh.

numerical and analytical solutions, which will help to evaluate the angular displacement (phase) errors produced by schemes.

The results of the experiments with the 99×99 grid points mesh, presented in Table II, show that the SL2T and the SL2TS schemes produced negative values larger (in magnitude) than the SL3T and the SL2S3T schemes after one revolution, which indicates that the latter schemes have less numerical dispersion than the others for shorter integration periods. For longer integrations, the SL3T scheme performed better than the others. Regarding the maximum values of ϕ, the SL3T and the SL2S3T schemes have about the same performance, which was better than for the SL2T and the SL2TS schemes.

The percentual loss of ϕ results show that the SL3T scheme has better 'mass' conservation than the others.

The ratio between the sums of squares of ϕ show that for Courant numbers 1.0 and 4.0 the SL3T and the SL2S3T schemes produced similar results, both better than the SL2T scheme. However, for Courant number 10.0 the SL2S3T scheme performed better than the other schemes. The errors produced by the SL2TS scheme are smaller only for Courant number 4.0.

DOI: 10.1002/fld

Table II. Maximum and minimum values of the ϕ function, conservation properties, and correlation between analytical an numerical solutions, after one and 10 revolutions of the Gaussian hill in experiments with Courant number equal to 1.0, 4.0 and 10.0 with the 99×99 grid points mesh.

Scheme	ϕ_{MAX} ($\times 10^5$)	ϕ_{MIN} ($\times 10^4$)	$100 \times [1 - (\sum \phi_{ij} / \sum \phi_{ij}(0))]$ (%)	$\sum \phi_{ij}^2 / \sum \phi_{ij}^2(0)$	Correlation
Results after 1 revolution					
Courant number = 1					
Eulerian	0.266	−1.750	−0.768E+00	1.007	0.257
SL2T	0.313	−0.180	0.158E−01	0.407	0.800
SL2TS	0.313	−0.180	0.177E−01	0.407	0.800
SL3T	0.345	−0.162	0.129E−02	0.441	0.827
SL2S3T	0.345	−0.162	0.956E−02	0.441	0.827
Courant number = 4					
SL2T	0.503	−0.170	0.328E+00	0.605	0.919
SL2TS	0.549	−0.182	−0.101E+02	0.729	0.915
SL3T	0.597	−0.135	0.820E−01	0.701	0.951
SL2S3T	0.600	−0.132	0.137E+00	0.700	0.954
Courant number = 10					
SL2T	0.577	−0.189	−0.140E+02	0.750	0.928
SL2TS	0.584	−0.142	0.666E+00	0.702	0.954
SL3T	0.732	−0.085	−0.636E−02	0.814	0.953
SL2S3T	0.696	−0.141	−0.831E+01	0.834	0.971
Results after 10 revolutions					
Courant number = 1					
SL2T	0.116	−0.082	0.223E+00	0.158	0.538
SL2TS	0.116	−0.082	0.190E+01	0.158	0.537
SL3T	0.129	−0.083	−0.776E−01	0.177	0.565
SL2S3T	0.129	−0.083	0.297E−02	0.176	0.565
Courant number = 4					
SL2T	0.201	−0.177	0.806E+01	0.261	0.686
SL2TS	0.267	−0.157	−0.316E+02	0.463	0.676
SL3T	0.260	−0.114	0.823E+00	0.337	0.660
SL2S3T	0.260	−0.180	0.652E+01	0.336	0.741
Courant number = 10					
SL2T	0.293	−0.195	−0.490E+02	0.578	0.635
SL2TS	0.261	−0.168	0.108E+02	0.323	0.717
SL3T	0.362	−0.131	0.875E−01	0.462	0.101
SL2S3T	0.366	−0.210	−0.347E+02	0.633	0.712

The correlation values give an indication of the phase errors of the simulations. It can be seen that as the Courant number increases the correlations increase for short periods of integration for all schemes. On the other hand, for longer integrations the SL3T scheme shows significantly smaller correlations for longer time steps. In all cases, the SL2S3T scheme shows higher correlation values than the other schemes, except for 10 revolutions with Courant number 10.0, where the SL2TS scheme was slightly better.

Figure 4 shows analytical and numerical solutions after 10 revolutions of the Gaussian hill in the 99×99 grid points mesh, for the experiment with Courant number equal to 4.0. The hill center positions simulated by the SL2T, the SL2TS, and the SL2S3T schemes are closer to the

DOI: 10.1002/fld

Table III. Maximum and minimum values of the ϕ function, conservation properties, and correlation between analytical an numerical solutions, after one and 10 revolutions of the Gaussian hill in experiments with Courant number equal to 1.0, 4.0 and 10.0 with the 67×67 grid points mesh.

Scheme	ϕ_{MAX} ($\times 10^5$)	ϕ_{MIN} ($\times 10^4$)	$100 \times [1 - (\sum \phi_{ij} / \sum \phi_{ij}(0))]$ (%)	$\sum \phi_{ij}^2 / \sum \phi_{ij}^2(0)$	Correlation
Results after 1 revolution					
Courant number = 1					
Eulerian	0.324	−1.928	−0.289E+01	1.007	0.322
SL2T	0.363	−0.199	0.231E−01	0.464	0.839
SL2TS	0.363	−0.199	0.328E−01	0.464	0.839
SL3T	0.399	−0.173	0.333E−02	0.502	0.864
SL2S3T	0.399	−0.173	0.155E−01	0.502	0.864
Courant number = 4					
SL2T	0.555	−0.164	0.857E+00	0.662	0.943
SL2TS	0.544	−0.152	0.206E+01	0.632	0.940
SL3T	0.660	−0.119	−0.126E−01	0.756	0.968
SL2S3T	0.652	−0.116	0.461E+00	0.753	0.970
Courant number = 10					
SL2T	0.645	−0.111	0.398E+01	0.731	0.963
SL2TS	0.652	−0.112	0.201E+01	0.749	0.969
SL3T	0.780	−0.063	−0.237E+00	0.858	0.918
SL2S3T	0.761	−0.062	0.199E+01	0.835	0.986
Results after 10 revolutions					
Courant number = 1					
SL2T	0.138	−0.099	0.688E+00	0.187	0.580
SL2TS	0.138	−0.999	0.158E+01	0.187	0.579
SL3T	0.155	−0.098	0.838E+00	0.210	0.609
SL2S3T	0.155	−0.099	0.953E+00	0.209	0.609
Courant number = 4					
SL2T	0.227	−0.142	−0.196E+02	0.335	0.680
SL2TS	0.223	−0.161	0.351E+01	0.287	0.702
SL3T	0.305	−0.120	−0.101E+00	0.392	0.732
SL2S3T	0.295	−0.157	0.619E+01	0.385	0.784
Courant number = 10					
SL2T	0.275	−0.117	0.333E+02	0.237	0.447
SL2TS	0.296	−0.123	0.193E+02	0.314	0.691
SL3T	0.422	−0.137	−0.129E+01	0.534	−0.023
SL2S3T	0.385	−0.133	0.185E+02	0.399	0.714

analytical solution than the position obtained with the SL3T scheme. The spreading of the hill is more significant in the SL2T and the SL2TS solutions, whereas the SL3T and the SL2S3T solutions showed similar distributions of the ϕ field. All schemes approximately preserved the circular shape of the Gaussian hill.

Table III presents numerical results of the simulation with the 67×67 grid points domain, which has flow trajectories with curvatures greater than those of the 99×99 grid points mesh. The SL2T and the SL2TS schemes showed less numerical dispersion than the SL3T and the SL2S3T schemes after 10 revolutions in the simulation with Courant number 10.0. In all other cases they

DOI: 10.1002/fld

Table IV. Maximum and minimum values of the ϕ function, conservation properties, and correlation between analytical an numerical solutions, after one and 10 revolutions of the Gaussian hill in experiments with Courant number equal to 1.0, 4.0 and 10.0 with the 33×33 grid points mesh.

Scheme	ϕ_{MAX} ($\times 10^5$)	ϕ_{MIN} ($\times 10^4$)	$100 \times [1 - (\sum \phi_{ij} / \sum \phi_{ij}(0))]$ (%)	$\sum \phi_{ij}^2 / \sum \phi_{ij}^2(0)$	Correlation
Results after 1 revolution					
Courant number = 1					
Eulerian	0.482	−2.320	−0.191E+01	1.006	0.469
SL2T	0.474	−0.219	−0.587E+00	0.581	0.903
SL2TS	0.474	−0.220	−0.611E+00	0.581	0.902
SL3T	0.513	−0.181	−0.270E+00	0.621	0.922
SL2S3T	0.513	−0.182	−0.372E+00	0.621	0.922
Courant number = 4					
SL2T	0.664	−0.131	0.270E+01	0.737	0.972
SL2TS	0.665	−0.130	0.840E+00	0.749	0.972
SL3T	0.735	−0.084	−0.125E+00	0.841	0.979
SL2S3T	0.752	−0.082	0.126E+01	0.828	0.987
Courant number = 10					
SL2T	0.744	−0.797	0.171E+02	0.698	0.936
SL2TS	0.717	−0.712	0.793E+01	0.775	0.972
SL3T	0.851	−0.027	−0.339E+01	0.951	0.625
SL2S3T	0.794	−0.031	0.903E+01	0.831	0.976
Results after 10 revolutions					
Courant number = 1					
SL2T	0.190	−0.139	−0.515E+01	0.248	0.668
SL2TS	0.190	−0.139	−0.562E+01	0.249	0.667
SL3T	0.215	−0.130	−0.703E+01	0.284	0.695
SL2S3T	0.215	−0.131	−0.640E+01	0.282	0.697
Courant number = 4					
SL2T	0.269	−0.124	0.194E+02	0.270	0.788
SL2TS	0.287	−0.128	0.621E+01	0.329	0.803
SL3T	0.391	−0.135	−0.509E+01	0.500	0.536
SL2S3T	0.368	−0.133	0.953E+01	0.415	0.859
Courant number = 10					
SL2T	0.160	−0.078	0.854E+02	0.032	−0.016
SL2TS	0.274	−0.118	0.572E+02	0.148	0.286
SL3T	0.568	−0.125	−0.427E+02	0.959	−0.035
SL2S3T	0.365	−0.162	0.609E+02	0.186	0.172

produced larger (in magnitude) negative values. The differences between the results of the SL3T and the SL2S3T schemes were less significant than in the case of the 99×99 grid points domain. In general, the results were better in the greater curvature domain.

The SL3T and the SL2S3T solutions had better 'mass' conservation properties than the SL2T ones, with a slightly better performance of the SL3T scheme for one revolution. In general the 'mass' loss (values >0) and 'mass' creation (values <0) errors were larger (in magnitude) in this domain than those obtained for the 99×99 grid points mesh. For longer integrations none of the schemes was clearly better than the others.

DOI: 10.1002/fld

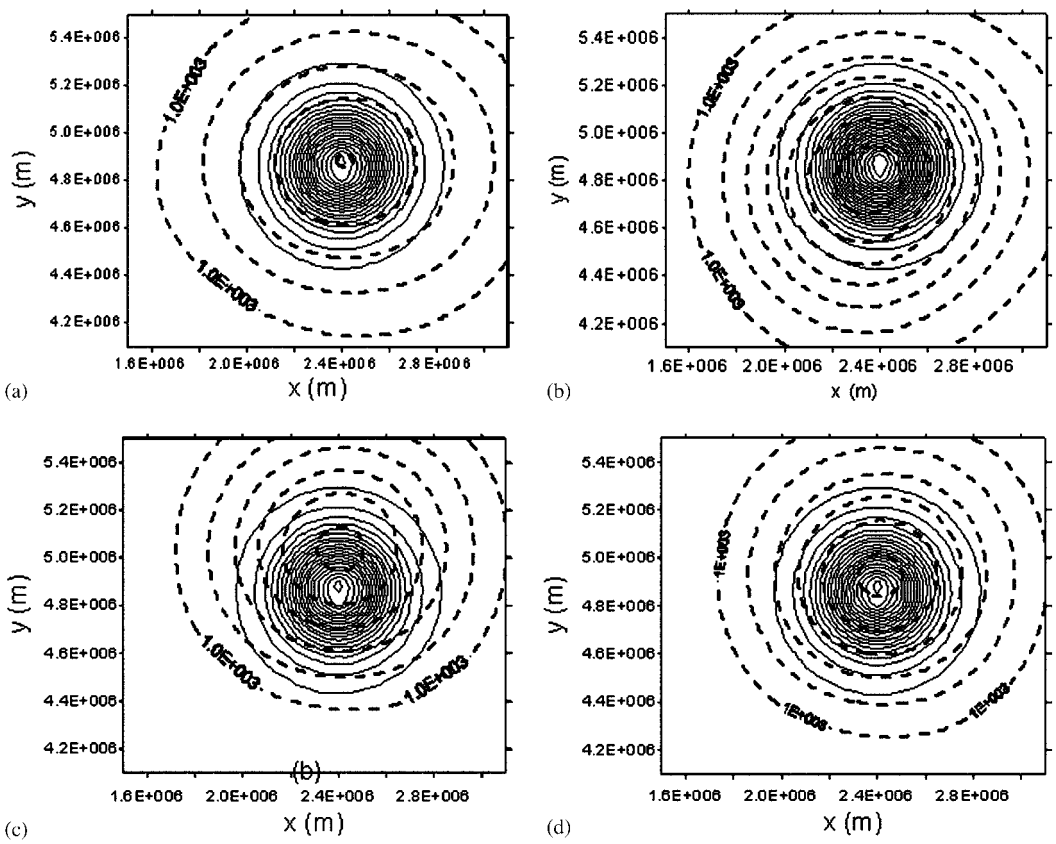

Figure 4. Analytical (solid lines) and numerical (dashed lines) solutions using the SL2T scheme (a), the SL2TS scheme (b), the SL3T scheme (c) and the SL2S3T scheme (d) after 10 revolutions of the Gaussian hill, for the experiments with the 99×99 grid points mesh with time step set to produce Courant number equal to 4.0.

The SL3T and the SL2S3T schemes presented smaller damping of the solution than the SL2T and the SL2TS schemes.

The correlations of the analytical and the numerical solutions for the experiments with Courant numbers equal to 1.0 and 4.0 showed improvement in comparison with the results of the experiments with the 99×99 grid points domain. However, in the experiments with Courant number equal to 10.0 the SL3T scheme presented correlation values significantly lower than those for the larger domain. The SL2S3T scheme performed equally or better than the other schemes in all cases.

Figure 5 shows the analytical and numerical solutions obtained after 10 revolutions of the Gaussian hill with Courant number equal to 4.0. It can be seen that the SL3T solution shows better preservation of the shape of the Gaussian hill, with less spatial spreading, although the positioning of the hill center had larger errors than the other three schemes. Both the SL2T and the SL2S3T solutions presented 'tails' with larger spatial errors in the former. Except for the 'tail' the spatial spreading of the hill in the SL3T and the SL2S3T solutions was similar.

DOI: 10.1002/fld

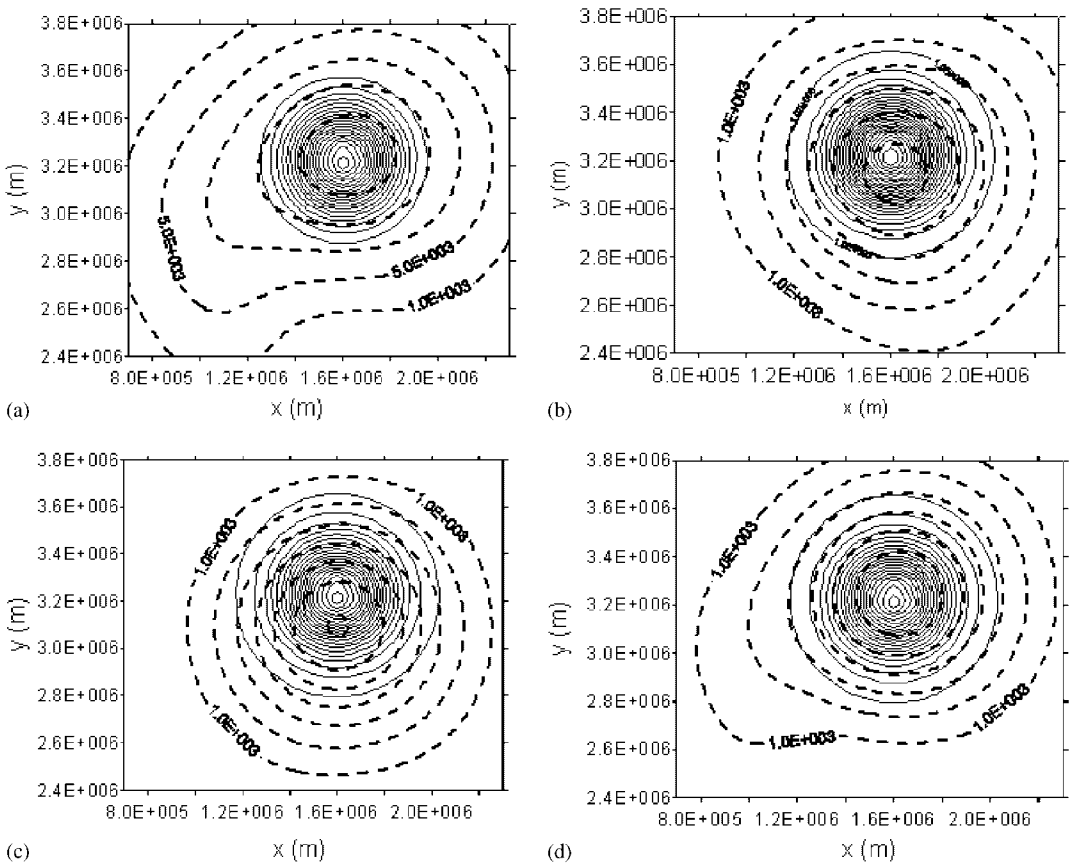

Figure 5. Analytical (solid lines) and numerical (dashed lines) solutions using the SL2T scheme (a), the SL2TS scheme (b), the SL3T scheme (c) and the SL2S3T scheme (d) after 10 revolutions of the Gaussian hill, for the experiments with the 67×67 grid points mesh with time step set to produce Courant number equal to 4.0.

Numerical results of the simulations in the 33×33 grid points grid, with more strongly curved flow trajectories, are presented in Table IV. The SL2T scheme produced larger numerical dispersion after one revolution, but equal or smaller dispersion after 10 revolutions than the other two schemes. The SL3T performed better than the SL2S3T scheme, especially in the case with $C = 10.0$ after 10 rotations. The results were in general better in this case than those for the 67×67 grid points domain.

The SL3T scheme had better 'mass' conservation after one revolution for all Courant numbers. After 10 revolutions the SL3T solutions were in general better than those of the other schemes.

After one revolution the amplitude preservation improves with increasing Courant number whereas after 10 revolutions it improves with increasing Δt only for the SL3T scheme. The results are in general better in this domain than in the larger ones. The three-time level schemes performed better than the two-time level ones.

The SL2S3T scheme produced equal or better correlation values than the other schemes in all cases, except for 10 revolutions with Courant number 10.0, where the SL2TS scheme had better

DOI: 10.1002/fld

performance. For increasing Δt the SL3T scheme was the one that showed greater growth of phase errors.

Figure 6 shows the analytical and the numerical solutions with $C = 4.0$ after 10 revolutions of the Gaussian hill in the 33×33 grid points mesh. In this case with larger flow curvatures the SL2S3T performed better than the other schemes, with good shape preservation, less spatial spreading of the hill and better positioning of the hill center. The SL3T solution was the one with greater error in the positioning of the hill center.

In all domains the Eulerian solution presented greater numerical dispersion and phase errors than the semi-Lagrangian schemes. Except for the 33×33 grid points mesh at Courant number equal to 1.0, the Eulerian method presented larger 'mass' conservation errors than all semi-Lagrangian schemes. However, it produced better (average) amplitude conservation than the semi-Lagrangian schemes for all cases. This is due to the fact that the spatial interpolation procedure of the

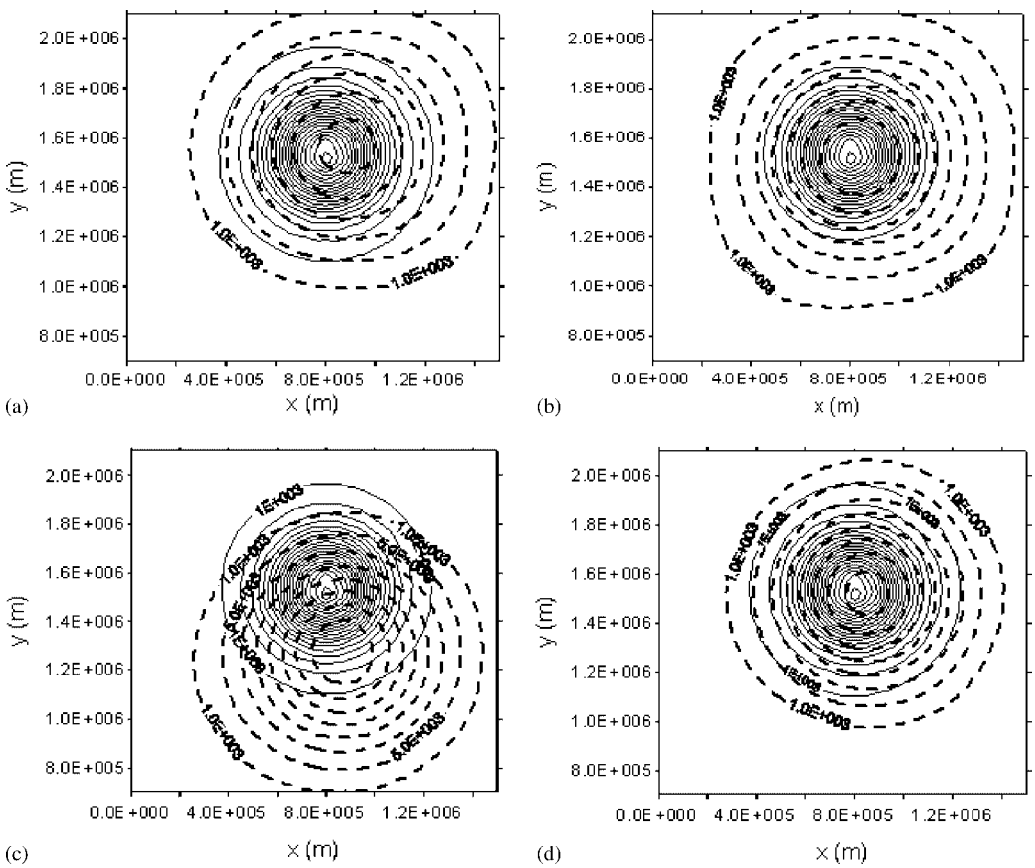

Figure 6. Analytical (solid lines) and numerical (dashed lines) solutions using the SL2T scheme (a), the SL2TS scheme (b), the SL3T scheme (c) and the SL2S3T scheme (d) after 10 revolutions of the Gaussian hill, for the experiments with the 33×33 grid points mesh with time step set to produce Courant number equal to 4.0.

DOI: 10.1002/fld

semi-Lagrangian schemes causes damping of the solution. Higher-order interpolations could reduce the damping. However, such interpolations, in general, have a higher computational cost.

4.2. Non-linear advection experiments

The conservation properties of the semi-Lagrangian schemes will be assessed by running experiments in domains defined by $\mathrm{NX} \times \mathrm{NY}$ grid points along the x and y directions, respectively, where the initial condition is set by the following streamfunction, which has the same functional form of the one used by Arakawa and Lamb [14]:

$$\psi_{i,j} = \Psi \sin\left(\frac{\pi \cdot i}{nx}\right)\left[\cos\left(\frac{\pi \cdot j}{2 \cdot ny}\right) + 0.1 \cos\left(\frac{\pi \cdot j}{ny}\right)\right] \tag{34}$$

where Ψ is the amplitude (constant); $nx = \mathrm{NX} - 1$; $ny = (\mathrm{NY} - 1)/2$; i: 0, nx; j: $-ny$, ny; and $\psi = 0$ along the boundary.

All domains have uniform grid spacing $\Delta x = \Delta y = 5000\,\mathrm{m}$ and $\mathrm{NX} = 129$. Three experimental domains were set with different values for NY: 129 for the smaller curvature case; 97 for the medium curvature case and 65 for the larger curvature case. The amplitude Ψ was adjusted in each case in order to keep the maximum speed between 10.5 and 11.5 m/s. Figure 7 shows the three initial streamfunctions for the non-linear advection experiments.

Control runs for the three domains were performed, with the use of the *leapfrog* scheme and the Arakawa discretization scheme (Equation (28a)) to solve the Eulerian form of the relative vorticity

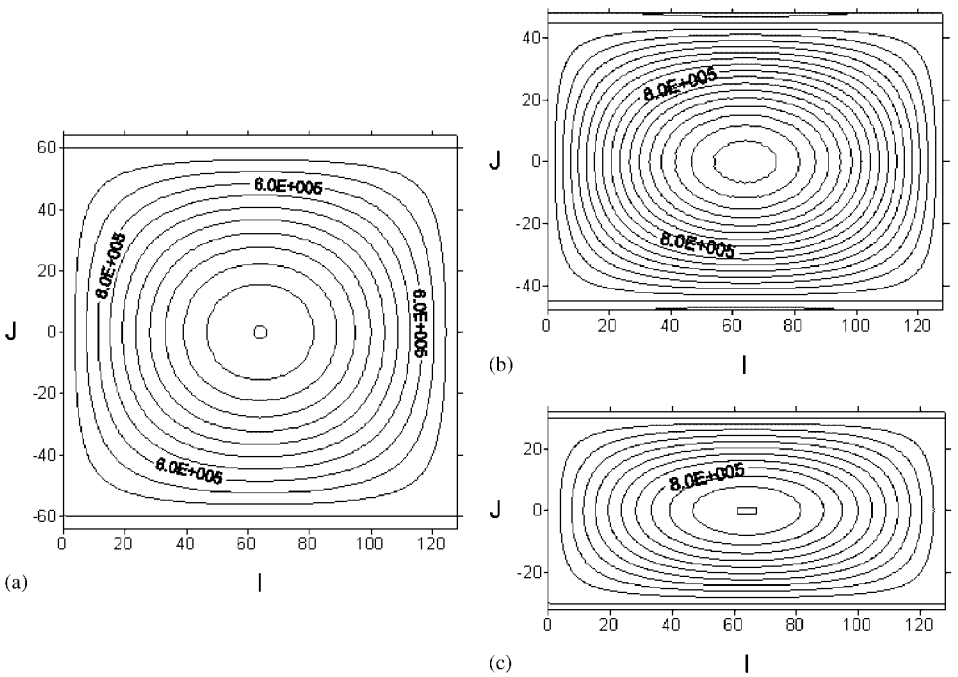

Figure 7. Initial streamfunction fields for the non-linear advection experiments: 129×129 grid points mesh (a), 129×97 grid points mesh (b), and 129×65 grid points mesh (c).

DOI: 10.1002/fld

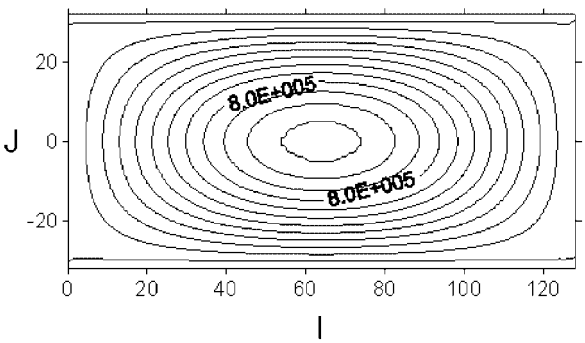

Figure 8. Final streamfunction field (30 days integration time) for the non-linear advection experiment with the 129×65 grid points mesh, using the Eulerian leapfrog method.

conservation Equation (25), for an integration time of 30 days, with Δt set to obtain Courant number $C = 0.6$. It is important to point out that even with the use of the Arakawa discretization scheme, non-linear instability caused by aliasing could be controlled only for Courant number as small as 0.6. With time steps larger than that the simulation 'blew up' before completing two days of integration time. The use of a high-frequency time filter such as the Robert-Asselin filter [17] or the inclusion of explicit diffusion terms in the governing equations [18] could help to control the non-linear instability. However, in this study we are just interested in producing a solution to be used as reference for the semi-Lagrangian experiments. Figure 8 shows the final streamfunction field for the 129×65 grid points mesh. It can be seen that, except for some damping of the maximum at the domain center, there is no significant change in the shape of the streamfunction after the 30 days integration. Figure 9 presents the temporal evolution of the domain averages of enstrophy, kinetic energy (per unit mass), and vorticity from simulations with the Eulerian scheme for the three domains. It can be seen that there is a reasonable conservation of those quantities along the integration period.

The experiments with the semi-Lagrangian schemes were performed to solve the relative vorticity conservation equation in its Lagrangian form (Equation (23)). Time step was adjusted to produce Courant numbers 0.6, 2.0, 4.0, 6.0, 8.0 and 10.0, respectively. The iteration procedure used to calculate the length of the particle displacement was the same used for the linear advection experiments. The integration time was 30 days. When the integration time reached 10, 20 and 30 days, domain averages of enstrophy, kinetic energy (per unit mass) and vorticity were calculated. After that, the ratios of those values to the corresponding values at the initial time were obtained. In a perfectly conserving scheme such a ratio should be equal to 1.0. Values greater than 1.0 indicate increase of the domain-averaged quantity, whereas values less than 1.0 indicate damping.

The results of the simulations are presented in Figures 10–12, where, for each Courant number and each numerical scheme, the three adjacent bars with the same filling pattern represent the ratios to the initial values of the averaged quantities, after 10, 20 and 30 days of integration (from the left to the right), respectively. In all experiments the values of the ratios to the initial value of the average enstrophy for the *leapfrog* scheme were equal to 1.0, showing that the scheme correctly conserves the domain-averaged enstrophy. For that reason, those results are not presented in the figures.

Figure 10 shows the results of the experiments for the 129×129 grid points mesh, which has smaller flow curvatures. The enstrophy bar chart (Figure 10(a)) shows that the semi-Lagrangian schemes have a similar performance for Courant numbers up to 4.0. As the Courant number

DOI: 10.1002/fld

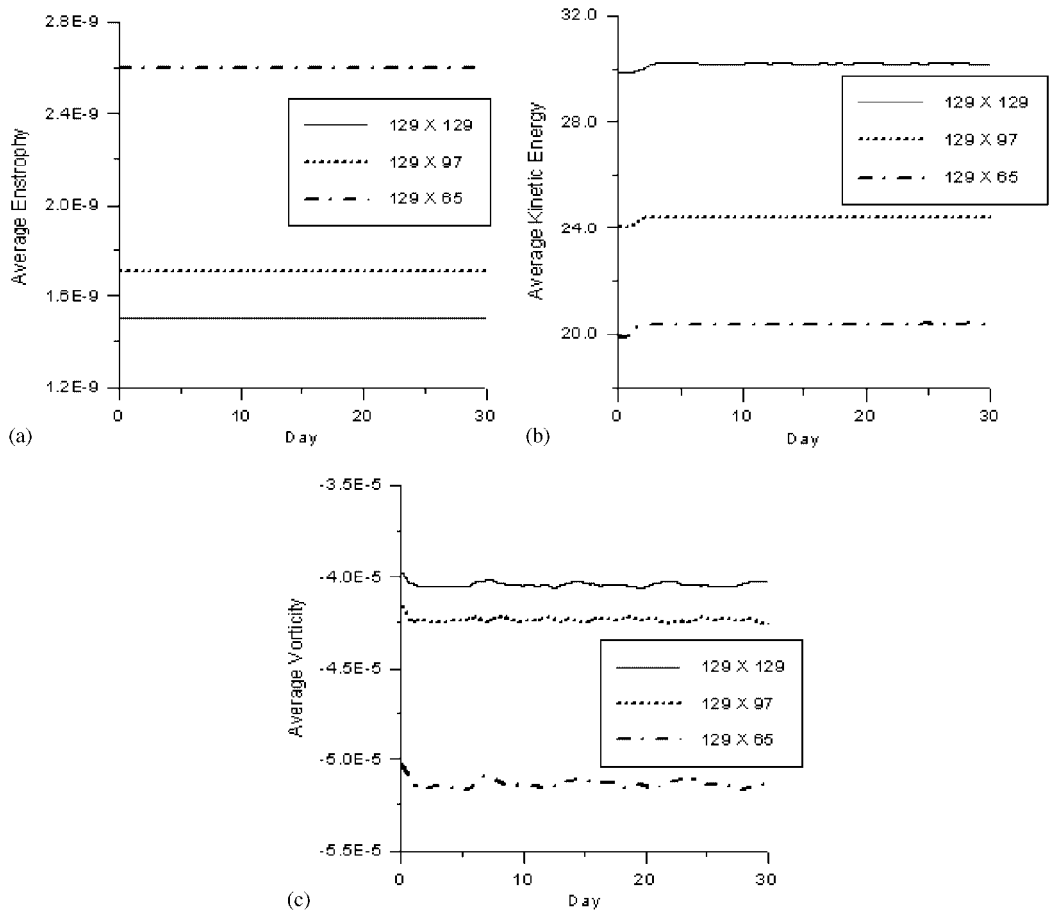

Figure 9. Temporal evolution of domain averaged enstrophy (a), kinetic energy per unit mass (b), and vorticity (c) with the use of the Eulerian leapfrog method, for the three computational domains: 129×129 grid points mesh (solid lines), 129×97 grid points mesh (dashed lines), and 129×65 grid points mesh (dot-dashed lines).

increases the errors of the SL2T, the SL2TS and the SL3T schemes increase continuously, whereas for the SL2S3T scheme there is no error growth for Courant numbers greater than 6.0. The SL2T and the SL2TS schemes start presenting significant error growth at Courant number 6.0. It is apparent that the SL3T scheme is more sensitive to cumulative errors at large Courant numbers, since the conservation errors increase significantly in time. The SL2S3T scheme, on the other hand, was the least sensitive to cumulative errors.

Figure 10(b) shows the kinetic energy conservation results. For $C = 0.6$ all methods produced similar errors. The SL2S3T scheme was less sensitive to increasing Courant number and cumulative errors than the other schemes. It performed equally or better than the other schemes for all Courant numbers, except 6.0, when the SL3T scheme produced smaller errors. The SL2T and the SL2TS schemes produce significant errors at $C = 6.0$, which increase with increasing time step. Again the SL3T scheme was the most sensitive to cumulative errors for $C = 10.0$.

DOI: 10.1002/fld

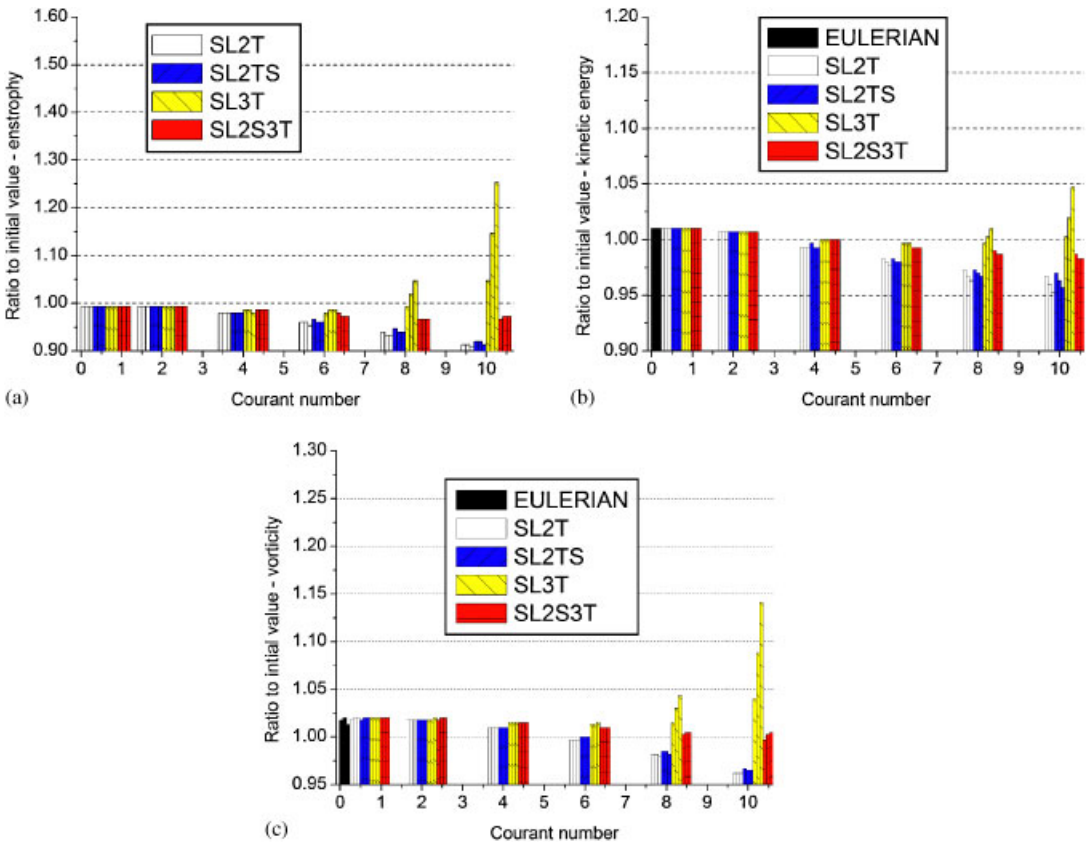

Figure 10. Ratio of domain averaged enstrophy (a), kinetic energy per unit mass (b), and vorticity (c) to the corresponding initial values, after 10, 20 and 30 days of integration time, for the 129×129 grid points mesh. Each bar filling pattern represents a different numerical scheme.

Figure 10(c) presents the vorticity conservation results for the experiments with the 129×129 grid points mesh. It can be seen that, except for $C = 6.0$, the SL2S3T scheme performed equally or better than the other schemes, especially for large Courant numbers. Again, the SL3T scheme was the most sensitive to increasing time step, at large Courant numbers, as well as to cumulative errors. Interestingly, the vorticity conservation errors of the SL2S3T scheme decrease for increasing Courant numbers. For all conservation quantities, the SL2T and the SL2TS schemes presented much larger errors than the SL2S3T scheme at $C = 10.0$.

Figure 11 shows the results for the experiments with the 129×97 grid points mesh, which has moderate flow curvature. The behavior of the enstrophy conservation errors (Figure 11(a)) was similar to that observed in the previous experiment, with the SL2S3T scheme performing equally or better than the other schemes, except for $C = 6.0$. The SL3T scheme showed larger errors in this domain than in the one with smaller flow curvature, whereas the SL2T, the SL2TS and the SL2S3T schemes did not present significantly larger errors in this case. However, similar to the previous case, the SL2T and the SL2TS schemes start presenting significant error growth at $C = 6.0$.

DOI: 10.1002/fld

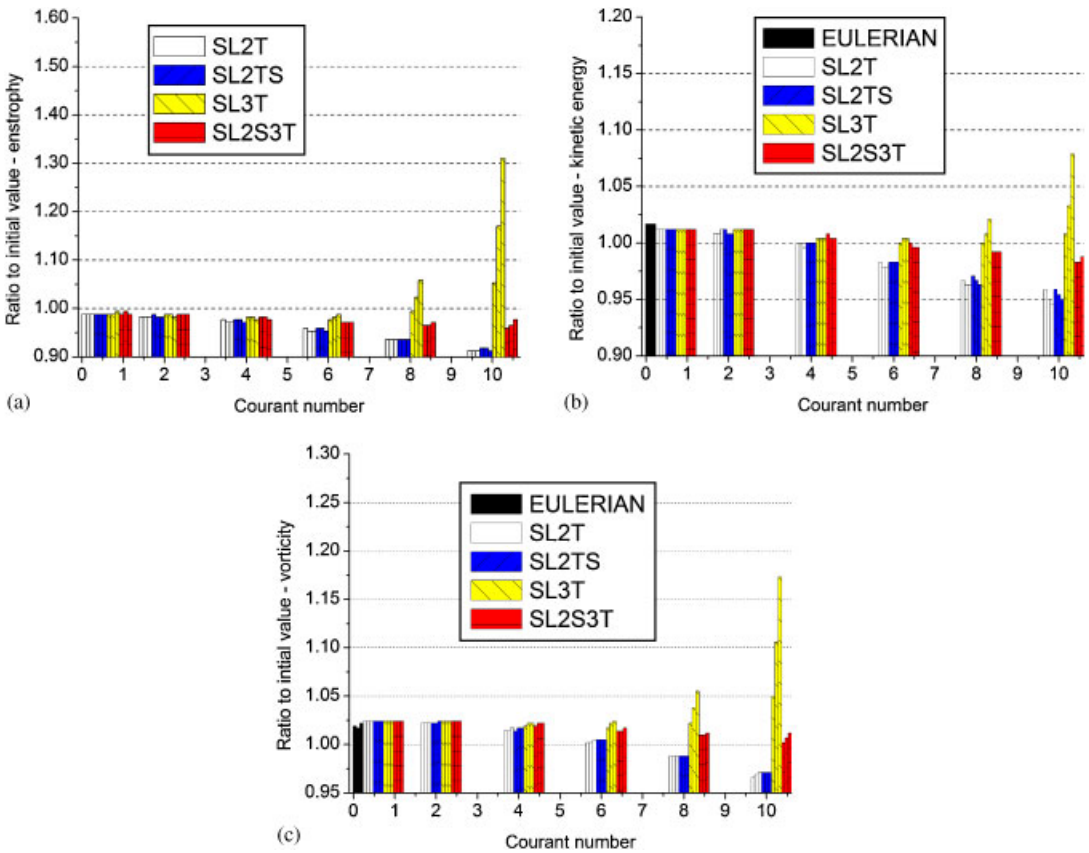

Figure 11. Ratio of domain averaged enstrophy (a), kinetic energy per unit mass (b), and vorticity (c) to the corresponding initial values, after 10, 20 and 30 days of integration time, for the 129×97 grid points mesh. Each bar filling pattern represents a different numerical scheme.

The kinetic energy conservation errors (Figure 11(b)) obtained for Courant number equal to 0.6 are slightly larger than those in the smaller flow curvature domain, with the Eulerian simulation producing larger errors than the semi-Lagrangian schemes. The SL2S3T scheme performed equally or better than the other schemes in all cases, and the two-time level and the SL3T schemes showed to be more sensitive to increasing time step as well as to cumulative errors. For this domain, the SL2T, the SL2TS and the SL2S3T schemes presented errors slightly larger than those of the first experiment, with the two-time level schemes producing large errors for Courant number equal or greater than 6.0. The SL3T scheme however produced much larger kinetic energy errors in this case.

The vorticity conservation errors results (Figure 11(c)) for the 129×97 grid points mesh have the same general behavior of the previous experiment, with the SL2S3T scheme performing equally or better than the other schemes for all cases, except for $C = 6.0$, where the SL2T and the SL2TS schemes produced better conservation. Again, the SL3T scheme showed to be highly sensitive to cumulative errors for large Courant numbers. The errors of the two-time level and the SL2S3T

DOI: 10.1002/fld

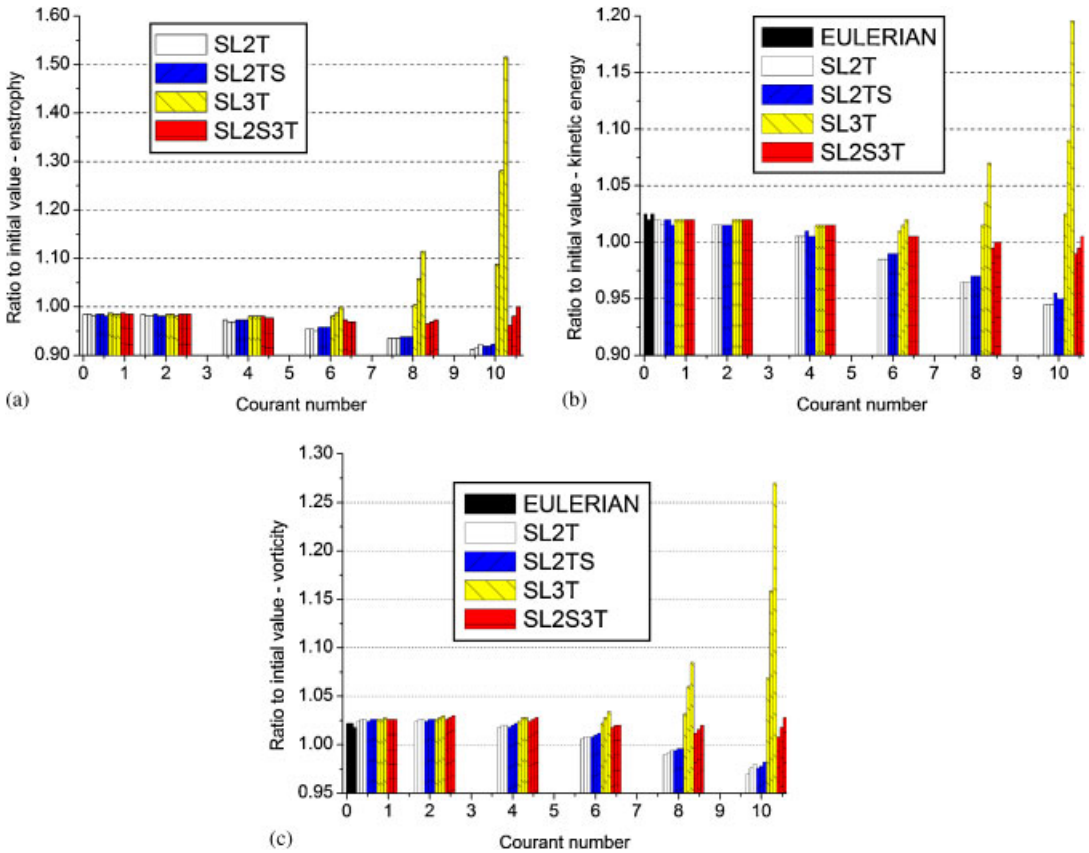

Figure 12. Ratio of domain averaged enstrophy (a), kinetic energy per unit mass (b), and vorticity (c) to the corresponding initial values, after 10, 20 and 30 days of integration time, for the 129×65 grid points mesh. Each bar filling pattern represents a different numerical scheme.

schemes were a little larger than in the first experiment, and the SL3T scheme produced much larger errors for this domain with moderate flow curvature. For the three averaged quantities, the SL2T and the SL2TS errors were much larger than those of the SL2S3T scheme for $C = 10.0$.

Figure 12 presents the results the results of the experiments with the 129×65 grid points mesh, which has stronger flow curvature. The general behavior of the numerical schemes was the same observed in the previous experiments. The most noticeable feature was that the SL2S3T scheme presented significantly smaller vorticity conservation errors for large Courant numbers in this case than in the previous ones. Except for enstrophy, the SL2S3T scheme showed equal or better conservation results than the Eulerian scheme, at all Courant numbers. The SL2T and the SL2TS schemes in this case also started showing significant sensitivity to increasing time step at Courant number 6.0. One more time the SL3T scheme showed to be highly sensitive to increasing Δt at large Courant numbers, as well as to cumulative errors. The SL2S3T scheme performed equally or better than the other semi-Lagrangian schemes at most Courant numbers, particularly the larger ones.

DOI: 10.1002/fld

4.3. Idealized frontogenesis experiments

The ability of the semi-Lagrangian schemes to represent strongly curved structures with sharp spatial gradients will be evaluated. The computational domain was set with 101×101 grid points, in the x and y directions, respectively, with grid spacing $\Delta x = \Delta y = 50$ non-dimensional units. Constant inflow, gradient outflow boundary conditions were applied along all boundaries [19].

Time step was set by calculating the maximum value of the tangential velocity V_T and then adjusting Δt to produce Courant numbers $C = 1.0$, 2.0, 4.0, 6.0, 8.0 and 10.0, respectively. The experiments were performed to produce six revolutions around the domain center of a fluid particle placed at the distance from the center with the maximum value of V_T.

The performances of the numerical schemes were evaluated by calculating the sum of the grid point values of the scalar field Q, which should equal zero in a perfectly antisymmetric solution. Also, the values of the magnitude of the gradient of the scalar field $|\nabla Q|$ at the domain central grid point were calculated. Its value should be a constant equal to 1.0 for all times, according to the analytic solution for the problem.

Figure 13 presents the solutions obtained for the idealized frontogenesis obtained with the use of the Eulerian (*leapfrog*) scheme, with $C = 1.0$. Figure 13(a) shows the initial Q field, and Figures 13(b), (c) and (d) show the scalar field after one, three and six revolutions, respectively. It can be seen that there is an increasing presence of numerical noise in the solution, with an almost complete loss of the spiral structure in the central part of the domain as the simulation advances in time.

Figure 14 presents the Q field after three revolutions, for the semi-Lagrangian solutions, with time step set for Courant number 4.0. There are no significant differences among the results, except for a slight smoothing of the central part of the Q field for the SL3T scheme (Figure 14(c)) as compared to the solutions obtained with the other schemes.

Figure 15 presents the temporal evolution of $|\nabla Q|$ at the domain center obtained for the simulations with the semi-Lagrangian schemes, for Courant number varying from 1.0 up to 10.0. It is expected that its value remains constant equal to 1.0 during the simulation. The graphs show that for all schemes $|\nabla Q|$ varies in time at the central grid point, due to the difficulty of the numerical solutions to handle the increasing scale-collapse that occurs due to the continuous inward spiraling of the Q field. The evolution of $|\nabla Q|$ for $C = 1.0$ is similar for all schemes. The two-time level schemes produce better results for Courant number 6.0, whereas the SL3T scheme solution is more accurate for $C = 2.0$ and the SL2S3T is better for $C = 4.0$. For Courant numbers 8.0 and 10.0 none of the schemes perform well, with the SL3T producing the least accurate results for those values of C.

Figure 16 presents the sum of final grid point values of Q after six revolutions. It is expected that this sum remains equal to zero along the simulation. All schemes produce negative values for the sum of Q, with the two-time level schemes producing the largest errors, for all Courant numbers. The three-time level schemes have similar performances. The decrease of the errors with increasing values of C is faster for the three-time level schemes than it is for the two-time level ones.

4.4. Computational cost

One of the most important advantages of the use of the semi-Lagrangian method is the possibility of using long time steps without the constraint of the CFL condition. However, the need for spatial and/or temporal interpolations of the semi-Lagrangian schemes imposes a computational overhead that must be assessed. We will analyze this aspect based on the processing speedup obtained by

DOI: 10.1002/fld

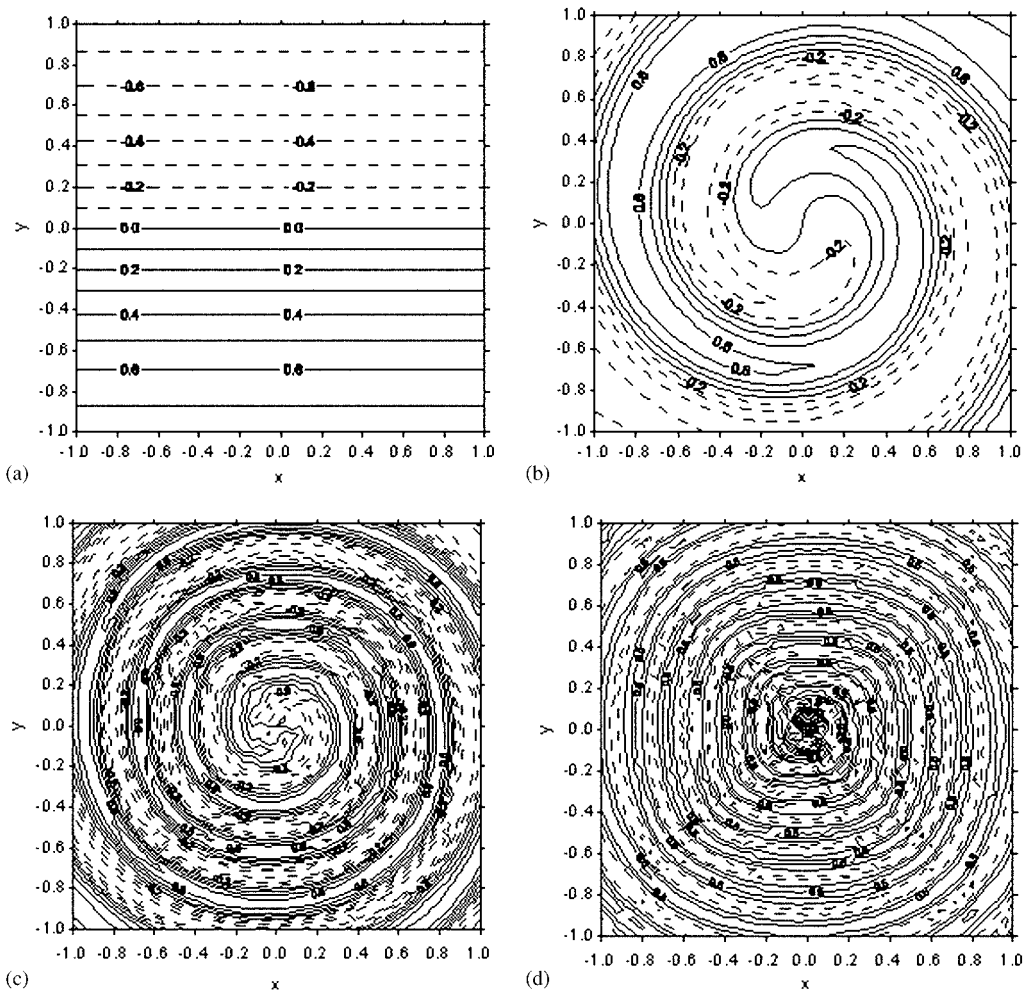

Figure 13. Initial condition (a) and Eulerian solutions of the idealized frontogenesis problem after one (b), three (c) and six (d) revolutions around the center. Dashed lines indicate negative values of Q.

the semi-Lagrangian schemes with respect to the Eulerian solutions. The processing speedup will be defined as the ratio between the CPU time consumed by the Eulerian solution at $C = 0.6$, and the CPU time consumed by a semi-Lagrangian solution. Values greater than 1.0 mean that the semi-Lagrangian scheme demands a smaller computational cost whereas values smaller than 1.0 mean that the Eulerian solution is more economical from a computational point of view.

Table V presents the processing speedup of the semi-Lagrangian schemes for the linear advection experiments, with the time step set to obtain Courant numbers equal to 1.0 and 10.0, respectively. It can be seen that for $C = 1.0$, the Eulerian solutions are much more economical than the semi-Lagrangian ones by a factor ranging from 4 to 10, approximately. The SL3T is the fastest semi-Lagrangian schemes, followed by the SL2T scheme and then by the SL2S3T and the SL2TS schemes. When the time step was set to produce $C = 10.0$, the SL2T and the SL3T schemes

DOI: 10.1002/fld

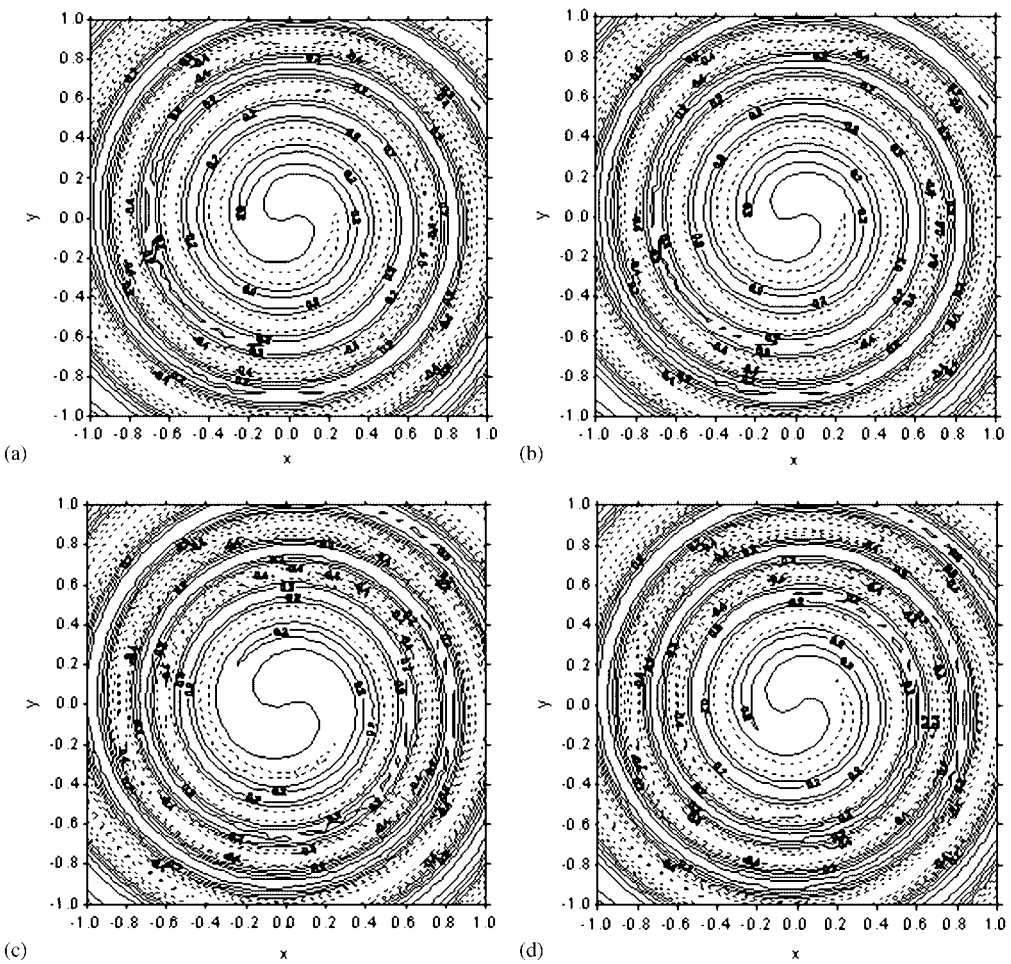

Figure 14. Semi-Lagrangian solutions of the idealized frontogenesis problem after four revolutions around the center using the SL2T scheme (a), the SL2TS scheme (b), the SL3T scheme (c) and the SL2S3T scheme (d), with time step set to produce Courant number equal to 4.0. Dashed lines indicate negative values of Q.

produced a very small speedup with respect to the Eulerian scheme. The computational cost of the SL2TS and the SL2S3T schemes remained greater than that of the Eulerian scheme, except for the 99×99 grid with $C = 10.0$ for the SL2TS scheme. However, it has to be considered that the Eulerian scheme produces, in general, much more numerical dispersion, with very large RMS and phase errors. In that case the additional computational cost of the semi-Lagrangian schemes is worthwhile since their solutions are more accurate.

The linear problem may not be an appropriate reference for evaluating the relative efficiency of the different schemes because the velocity field is constant in time. In the non-linear advection case, on the other hand, the u and v velocity components have to be calculated at each time step. Besides, the use of finite differences for spatial discretization makes necessary the

DOI: 10.1002/fld

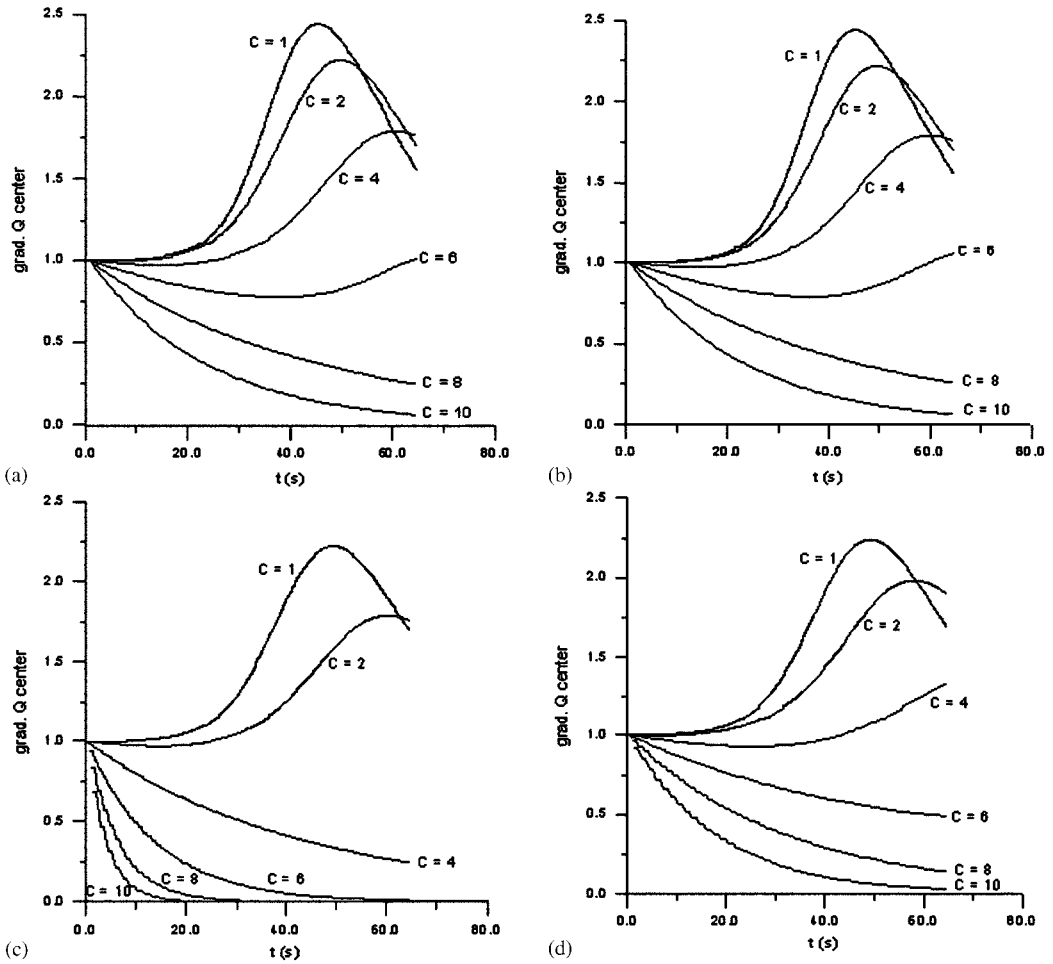

Figure 15. Temporal evolution of $|\nabla Q|$ at the central grid point using the SL2T scheme (a), the SL2TS scheme (b), the SL3T scheme (c) and the SL2S3T scheme (d), with time step set to produce Courant numbers ranging from 1.0 to 10.0.

use of some aliasing control technique to avoid non-linear instability of the Eulerian solution, which imposes a computational overhead on that scheme. This situation is more realistic than the linear advection case.

Figure 17 presents the processing speedup of the semi-Lagrangian schemes with respect to the Eulerian solutions for the non-linear advection experiments. For simplicity the values presented in the graph represent the average speedup for the three meshes, since the values did not vary much for each domain configuration. It can be seen that in the non-linear advection experiments, for Courant numbers as small as 4.0 the semi-Lagrangian schemes have a computational cost smaller than that of the Eulerian scheme. The SL3T scheme is the one that yields larger speedups, except for Courant number 10.0, where the SL2TS scheme was more efficient. The SL2T and the SL2S3T schemes yield about the same efficiency. In all cases the SL2TS scheme is more efficient than

DOI: 10.1002/fld

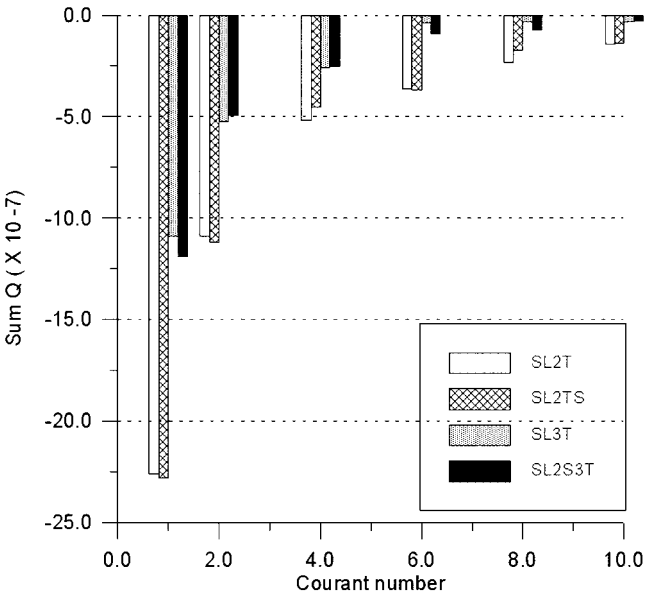

Figure 16. Sum of the final values of Q as a function of Courant number after six revolutions around the center. Each bar filling pattern represents a different semi-Lagrangian scheme.

Table V. Processing speedup of semi-Lagrangian schemes with respect to the Eulerian solution for experiments with Courant number equal to 1.0 and 10.0, with the three computational domains, for linear advection experiments.

Mesh	SL2T	SL2TS	SL3T	SL2S3T
Semi-Lagrangian scheme				
Courant number = 1.0				
33×33	0.10	0.07	0.20	0.08
67×67	0.12	0.07	0.23	0.09
99×99	0.15	0.10	0.28	0.12
Courant number = 10.0				
33×33	1.11	0.79	1.11	0.64
67×67	1.21	0.82	1.21	0.69
99×99	1.52	1.04	1.52	0.88

the SL2T and the SL2S3T scheme. Although the SL3T scheme is the one with larger speedups it is also the one that produces less accurate solutions for large Courant numbers. The two-time level schemes, on the other hand, are the ones that start producing errors larger than those of the Eulerian scheme at small Courant numbers. The SL2S3T scheme, in general, produces kinetic energy and vorticity errors equal or smaller than those of the Eulerian scheme both for small and large Courant numbers, even in the presence of strongly curved flow.

For the experiments of the idealized frontogenesis problem, the SL2S3T scheme, on the average, spent about 85% more computer time to run the experiments than the other semi-Lagrangian schemes, which had all about the same computational cost to produce the simulations.

DOI: 10.1002/fld

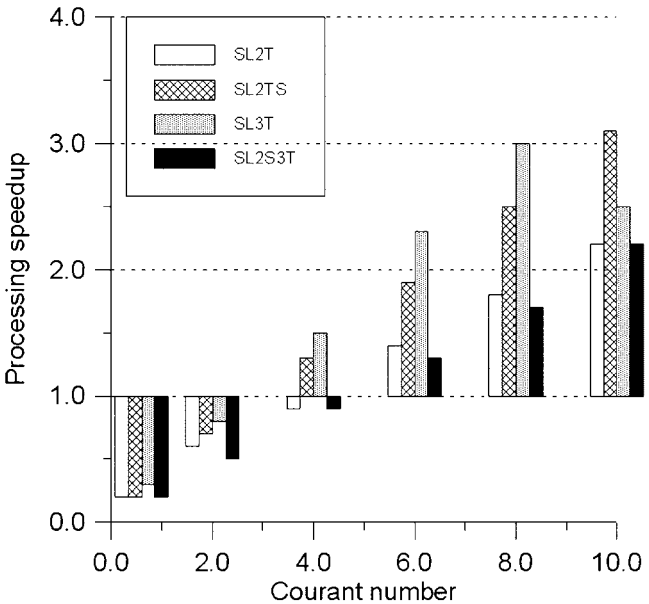

Figure 17. Average processing speedup of the semi-Lagrangian schemes with respect to the Eulerian leapfrog method. Each filling pattern represents a different semi-Lagrangian scheme.

5. DISCUSSION AND CONCLUSIONS

This work proposed a new two-step three-time level semi-Lagrangian scheme (SL2S3T) for calculation of particle trajectories. The scheme has $O(\Delta t^2)$ global time truncation error and is intended to yield accurate determination of particle departure points when using large time steps, especially in flows with significant curvature.

Experiments were performed both for linear and non-linear idealized advection problems as well as for an idealized frontogenesis problem. The results of the experiments with the SL2S3T scheme were compared with those obtained with the use of an Eulerian *leapfrog* scheme and three other semi-Lagrangian schemes: the three-time level scheme of Robert (SL3T), the two-time level scheme of MacDonald and Bates (SL2T) and the two-time level scheme of Hortal (SL2TS).

In the linear experiments a Gaussian hill was translated along circular paths with three different advection radii. The results showed that the SL2S3T scheme produced equal or smaller RMS errors than the other schemes, for all experiments. The SL3T scheme performed equal to the SL2S3T scheme only at small Courant numbers. The SL2T and the SL2TS schemes produced RMS errors larger than those of the SL2S3T scheme in most of the cases. The Eulerian solution was the one with larger RMS errors. The experiments showed that increasing flow curvatures yield larger RMS errors for all schemes.

Regarding accuracy and conservation of properties of the schemes, the experiments showed that in some cases either the two-time level schemes or the SL3T scheme performed better, but in those cases the SL2S3T scheme presented errors comparable to those of the other schemes. The most remarkable feature of the SL2S3T scheme was its high accuracy in the representation of the

DOI: 10.1002/fld

angular displacement of the Gaussian hill, which was superior to the other schemes in all cases, especially at large Courant numbers.

The non-linear advection experiments consisted of solving the relative vorticity conservation equation in three different domains, which were set to have different flow curvatures. The objective of those experiments was to assess the conservation properties of the semi-Lagrangian schemes. The experiments showed that all schemes produced larger errors for increasing flow curvatures. By and large, the SL2S3T scheme performed equally or better than the other schemes, both for small and moderate time steps. For large Courant numbers its performance was significantly better than those of the two-time level and the SL3T schemes. The errors produced by the SL2S3T scheme did not change much for increasing Courant number and, in some cases, decreased, due to the non-monotonic behavior of the error of semi-Lagrangian schemes with respect to time step size.

The computational cost of the semi-Lagrangian schemes was also evaluated. In the linear advection experiments the Eulerian solution was much more efficient than the semi-Lagrangian ones. However, the semi-Lagrangian solutions were far more accurate. In the non-linear advection cases the SL3T and the SL2TS schemes were the most efficient. However, both had larger errors than the SL2S3T scheme at large Courant numbers. The experiments showed that the use of the SL2S3T scheme with large time steps would not compromise the solution accuracy.

The idealized frontogenesis experiments showed that all semi-Lagrangian schemes produced better results than the Eulerian method. For the semi-Lagrangian schemes, the SL3T was the one that produced the least accurate results regarding the conservation of the central gradient. The three-time level schemes produced more accurate global representation of the advected scalar field than the two-time level schemes.

The results of this study showed that the most relevant feature of the SL2S3T scheme is its robustness, since it consistently presents good performance both for small and large Courant numbers, in the presence of weakly as well as strongly curved flows as well as sharp gradients. Therefore, the two-step three-time level semi-Lagrangian scheme may be a good choice to obtain accurate numerical simulations at low computational cost, making it competitive with other presently used particle trajectory calculation schemes.

REFERENCES

1. Winn-Nielsen A. On the application of trajectory methods in numerical forecasting. *Tellus* 1959; **11**:180–196.
2. Sawyer JS. A semi-Lagrangian method of solving the vorticity advection equation. *Tellus* 1963; **15**:336–342.
3. Robert A. A stable numerical integration scheme for the primitive meteorological equations. *Atmosphere-Ocean* 1981; **19**:35–46.
4. Purser JR, Leslie LM. An efficient semi-Lagrangian scheme using third-order semi-implicit time integration and forward trajectories. *Monthly Weather Review* 1994; **122**:745–756.
5. Durran DR. *Numerical Methods for Wave Equations in Geophysical Fluid Dynamics*. Springer: New York, 1998; 303–331.
6. Falcone M, Ferreti R. Convergence analysis for a class of high-order semi-Lagrangian advection schemes. *SIAM Journal on Numerical Analysis* 1998; **35**:909–940.
7. Staniforth A, Côté J. Semi-Lagrangian integration schemes for atmospheric models—a review. *Monthly Weather Review* 1991; **119**:2206–2223.
8. Pudykiewicz J, Staniforth A. Some properties and comparative performance of the semi-Lagrangian method of Robert in the solution of the advection–diffusion equation. *Atmosphere-Ocean* 1984; **22**:283–308.
9. Kuo H, Williams RT. Semi-Lagrangian solutions to the inviscid Burgers equation. *Monthly Weather Review* 1990; **118**:1278–1288.
10. McDonald A, Bates JR. Improving the estimate of the departure point position in a two-time level semi-Lagrangian and semi-implicit scheme. *Monthly Weather Review* 1987; **115**:737–739.

DOI: 10.1002/fld

11. Bates JR, Semazzi FHM, Higgins RW, Barros SRM. Integration of the shallow water equations on the sphere using a vector semi-Lagrangian scheme with a multigrid solver. *Monthly Weather Review* 1990; **118**:1615–1627.
12. Hortal M. The development and testing of a new two-time-level semi-Lagrangian scheme (SETTLS) in the ECMWF forecast model. *Quarterly Journal of the Royal Meteorological Society* 2002; **128**:1671–1687.
13. Mahrer Y, Pielke RA. A test of an upstream spline interpolation technique for the advection terms in a numerical mesoscale model. *Monthly Weather Review* 1978; **106**:818–830.
14. Arakawa A, Lamb VR. Computational design of the basic dynamical processes of the UCLA general circulation model. In *Methods in Computational Physics—Volume 17*: *General Circulation Models of the Atmosphere*, Chang J (ed.). Academic Press: New York, 1977; 173–265.
15. Doswell CA. A kinematic analysis of frontogenesis associated with a nondivergent vortex. *Journal of the Atmospheric Sciences* 1984; **41**:1242–1248.
16. Davies-Jones R. Comments on 'A kinematic analysis of frontogenesis associated with a nondivergent vortex'. *Journal of the Atmospheric Sciences* 1985; **42**:2073–2075.
17. Haltiner GJ, Williams RT. *Numerical Prediction and Dynamic Meteorology*. Wiley: New York, 1980; 108–180.
18. Kantha LH, Clayson CA. *Numerical Models of Oceans and Oceanic Processes*. Academic Press: San Diego, 2000; 202–206.
19. Pielke RA. *Mesoscale Meteorological Modeling*. Academic Press: London, 1984; 363–368.

DOI: 10.1002/fld